

See discussions, stats, and author profiles for this publication at: <https://www.researchgate.net/publication/271197420>

# Fractal-Based Generative Design of Structural Trusses Using Iterated Function System

Article in *International Journal of Space Structures* · February 2015

DOI: 10.1260/0266-3511.29.4.181

CITATIONS

6

READS

1,085

2 authors:



**Iasef Md Rian**

University of Sharjah

19 PUBLICATIONS 53 CITATIONS

[SEE PROFILE](#)



**Mario Sassone**

bS-design

48 PUBLICATIONS 217 CITATIONS

[SEE PROFILE](#)

Some of the authors of this publication are also working on these related projects:



parametric design and computational morphogenesis of architectural structures and passive design in the field of architecture. [View project](#)



Parametric design, form finding and optimisation of shell, gridshell and spatial structures [View project](#)

**Fractal-Based Generative  
Design of Structural Trusses  
Using Iterated Function System**

*by*

**Iasef Md Rian and Mario Sassone**

*Reprinted from*

**INTERNATIONAL JOURNAL OF  
SPACE STRUCTURES  
Volume 29 · Number 4 · 2014**

**MULTI-SCIENCE PUBLISHING CO. LTD.**  
**5 Wates Way, Brentwood, Essex CM15 9TB, United Kingdom**

# Fractal-Based Generative Design of Structural Trusses Using Iterated Function System

Iasef Md Rian<sup>1</sup> and Mario Sassone<sup>2</sup>

Department of Architecture and Design (DAD), Politecnico di Torino, Viale Pier Andrea Mattioli, 39–10125, Turin, Italy, iasefrian@gmail.com<sup>1</sup>, mario.sassone@polito.it<sup>2</sup>

(Submitted on 16/09/2014, Reception of revised paper 20/12/2014, Accepted on 09/01/2015)

**ABSTRACT:** The purpose of this study is to apply the notion of fractal geometry in designing structural roof trusses. Fractal geometry, commonly characterized by the features of recursive self-similarity, is considered as a rule-based geometric system that can be generated by using the process of the Iterated Function System (IFS). Lattice configurations of conventional trusses generally show some extent of ‘self-similarity’ features that loosely and sometimes closely resemble with the properties of fractal shapes. The typical configurations of these regular trusses are strategically designed to provide adequate strength and stability to the structures for carrying enough vertical and wind loads. This paper, using the Iterated Function System based on Barnsely’s contraction mapping as a generative design method, proposes a new family of truss designs that follow the concept of fractal geometry. The Hausdorff dimensions and the Box Counting dimensions are evaluated to measure the fractality and detailness of the lattices of proposed fractal-based trusses. It also briefly investigates their mechanical properties for analyzing their practical feasibility in construction.

**Key Words:** truss design, fractal geometry, Iterated Function System, Hausdorff dimension, structural analysis

## 1. INTRODUCTION

In the field of construction, the geometric shapes or the assemblage of different geometric shapes plays a significant role in providing the strength, stability and safety as well as aesthetic appearance to the architectural and engineering structures. In the beginning of the 19th century, the systematic development of trusses and space-frame structures had appended a new construction component in architecture. Later, so far, the trusses have become a fundamental structural system that is widely used for constructing long-span, light-weight, high-rise and free-form structures. The reason behind the choice of structural

trusses for large and light structures is its light-weight lattice assembly, high stiffness and excellent mechanical behavior against both in compression and in tension. The mechanical behavior of a truss depends on the connecting patterns of different members inside the main outer frame, and most of these patterns follow regular and continuous geometric shapes, in the frame of Euclidean geometry, and only in very few recent cases, they assume more intricate shapes, somehow inspired by nonlinear mathematics and non-Euclidean geometries (Gawell, 2013).

Nevertheless, in nature and in mathematics, there exists another concept of geometry that is known as

\*Corresponding author e-mail: iasefrian@gmail.com

Fractal geometry. Fractal geometry, systematically first investigated and defined by Benoit Mandelbrot in the late 1970s, is commonly characterized by the property of self-similarity or self-affinity (Mandelbrot, 1983). It means, in a fractal shape, the replication of original or whole shape is contained into its parts. Besides, fractal geometry can explain and model many of the complex shapes and networks in nature that were uneasy to explain and reproduce by other regular and conventional geometric systems. Soon after its early development in the beginning of 1980s, fractal geometry has been applied to understanding and modeling the nonlinear and complex shapes in a list of different disciplines, ranging from science (Vicsek, 1992; Sornette, 2004; Peitgen, 2004) to engineering (Dekking, et. al., 1999; Leung, 2004, 2011) and medicine (Losa and Nonnenmacher, 2005) to arts (Wallace, 1996). In the field of built environment, its applications include architecture (Bovill, 1996; Ostwald, 2001; Rian, et. al., 2007), urban planning (Batty, 1985), landscape design (Milne, 1991), and so on. In the field of construction, so far, its applications are rare as compared to the other fields, especially by means of its application in designing structural shapes. As it has been mentioned before that the architectural and engineering structures are innately connected to their geometric shapes, hence, we can predict that fractal geometry may also be useful for designing the structural forms. This observation clearly gives us a hint about the efficacy of self-similar repetitions if we apply in truss design. The geometric configurations of structural trusses are usually the non-strict repetitions of self-similar curve assemblies. In some lattice structures, the hierarchical arrangement of members and their sub-members provide the strength and stiffness to the structures. In this context, with reference to the design of the Eiffel tower, Benoit Mandelbrot (1983) claimed in his seminal book *The Fractal Geometry of Nature*,

*"My claim is that (well before Koch, Peano, and Sierpinski), the tower that Gustave Eiffel built in Paris deliberately incorporates the idea of a fractal curve full of branch points. ... However, the A's and the tower are not made up of solid beams, but of colossal trusses. A truss is a rigid assemblage of interconnected submembers, which one cannot deform without deforming at least one submember. Trusses can be made enormously lighter than cylindrical beams of identical strength. And Eiffel knew that trusses whose 'members' are themselves subtrusses are even lighter."*

Mandelbrot's logical explanation of the geometric shape of such hierarchical or recursive self-similarity was termed by 'fractal', and accordingly, the potential application of fractal geometry can offer more refined geometry of such trusses that can be generated using some rule-based generative processes, such as Iterated Function System (IFS), and may provide better mechanical strength and innovative aesthetic appearance.

Regarding the mechanical properties of fractal-based structures, a recent research claims that a truss can be 'highly stiff', but 'ultra light' if fractal geometry principle is applied in designing its configuration (Rayneau-Kirkhope, et. al., 2010). Until now, very limited numbers of researches have been done to investigate the new forms generation of the architectural and engineering structures that are designed based on fractal geometry, and assess their mechanical properties. These investigations are limited within the designs and brief mechanical analyses of the fractal-based structural shapes such as treelike branching columns (Rian and Sassone, 2014), façade frame structures (Huylebrouck and Hammer, 2006) and shell structures (Rian and Sassone, 2014; Stotz, et. al., 2009; Vyzantiadou, et. al. 2006). There is also a very few studies in modeling and analyzing the structural roof trusses that follow fractal design principle (Epstein and Adeeb, 2008; Kishimoto and Natori, 2000). These investigations have proposed only a couple of designs of fractal-based trusses that are derived from known fractal shapes such as Sierpinski triangle (Kishimoto and Natori, 2000) and Koch curve (Epstein and Adeeb, 2008). Nevertheless, there is a potential possibility to introduce plentiful variety of new lattice configurations of trusses that follow the notion of fractal geometry. As far as known, Asayama and Mae (2002, 2004) were the first who proposed a new fractal shape for designing a structural truss. They used F.M. Barnsley's (1988) *contraction mapping* method for the automatic construction of a fractal shape for a layered arch design and a roof truss design and the evaluations of their Hausdorff dimensions. They also briefly analyzed the mechanical characteristics of their fractal truss and compared it with Kingpost truss. However, apart from this example which was attempted a decade ago in 2004, there have been no new research attempts on this particular topic to expand the possibility of designing a variety of new fractal-based trusses.

Therefore, the main objective of this study is to propose a list of new structural trusses by applying the

concept of fractal geometry, focusing on the design of pitched roof trusses. The core strategy is to expand the feasibility of new shape of truss structures by using a rule-based design development process supported by fractal geometry. For this purpose, our investigation proposes some fractal-based trusses as the non-conventional new designs, and some fractal-based trusses as the geometric refinement of conventional truss designs. Similar as Asayama and Mae's approaches (2002, 2004), the Iterated Function System (IFS) based on Barnsley's *contraction mapping* method (1988) are used in this study as a generative design tool for the automatic forms generation of fractal-based trusses and for the calculations of their Hausdorff dimensions. The Box Counting dimensions are calculated to measure the detailness of the internal lattices of the fractal-based trusses. The finitely iterated geometric models of all the proposed fractals are transformed into the finite element models of fractal-based trusses for their finite element analyses, and the results have been discussed to assess their structural characteristics.

## 2. THE TRUSSES AND THEIR SELF-SIMILARITY FEATURES

### 2.1. The early design of trusses and their development

The history of the design of structural trusses can be traced back to the construction of pitched roof trusses in the Roman period. In the earlier times, often an overall shape of a triangle was used for constructing a wooden roof frame. Sometimes, one post was added under a pair of two rafters for low-pitched or long-span roof. This post, traditionally known as crown post, was rested on the centre of a tie beam which could take upper loads. In this situation, the rafters and the post acted as compression members (Figure 1a) (Rinke and

Kotnik, 2010). Sometimes, the beam was made gentle upward curve to prevent sagging from the upper loads transformed by the crown post. The abstract detail of this frame system is shown in 'Figure 1a'. Surviving example of such crown post truss is seen in the 12th century St Clement Church roof at Old Romney in Kent, England. (Figure 1b).

Later, the Romans invented a new structural system in the same truss design, but by modifying the details and the mechanical principle of the system. Romans did not rest the vertical post on the tie beam. Instead, they attached the tie beam with the post that was anchored at the ridge where two rafters met. Thus, the vertical post became a hanging post, and acted as a tension member (Figure 2a) (Yeomans, 1992). An example of traditional king post is seen in the 18th century Bolduc House in Ste. Geneviève in Missouri (Figure 2b).

Therefore, a crown post was designed to be in a compression and transfers weight to the tie beam, while a king post was designed to be in tension and supports the tie beam. This technical improvement by means of mechanics of truss system had advanced the history of truss development in the later periods.

In the later periods, diagonal members were added to the truss designs so that the diagonals can transfer the vertical and horizontal loads. Apart from transferring the loads, the major role of diagonals were stiffening the truss structure, especially for the long-span trusse. Struts were added further in a regular pattern as posts to provide a robust structure. For long-span structures, more members were added depending on the bearing capacity and required stiffness, and formed a denser lattice configuration. After the Renaissance period, in Europe, different configurations of lattice patterns were seen in long-span truss designs

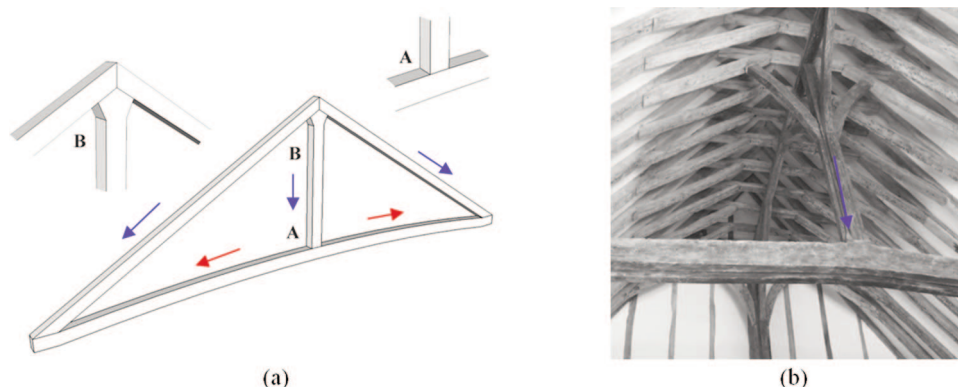


Figure 1. (a) A vertical post under compression traditionally known as 'crown post' standing on a tie beam, (b) An example of crown post in St Clement Church roof, Old Romney, Kent, England. (12th century).



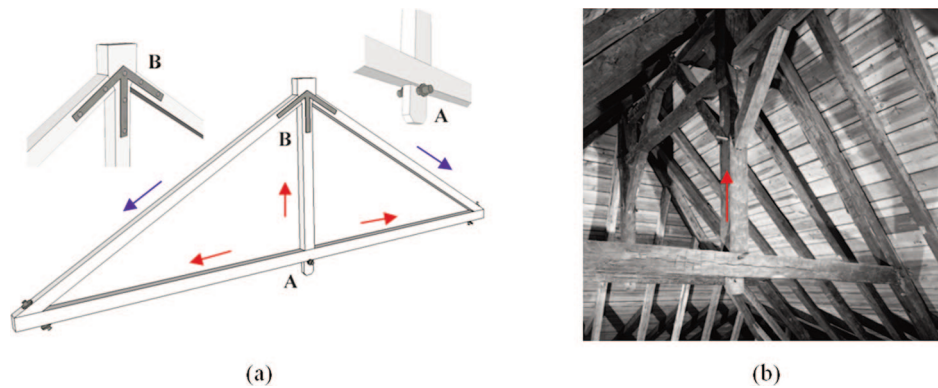


Figure 2. (a) A vertical post under tension traditionally known as ‘king post’ hanging from the joint of two rafters and hold the tie beam (b) An example of king post in the Bolduc House in Ste. Geneviève, Missouri (18th century).

depending on the requirements and applied loads. Since the 19<sup>th</sup> century, when steel has become popular and affordable in construction, several different varieties of truss systems started to appear and a list of engineers introduced some innovative truss system having unique lattice configurations to fill the interior of the main frame using the tension diagonals, compression struts and posts for increasing strength, stability and stiffness of the trusses (Calvert, 2004). Today, all of these trusses are considered as the standard trusses widely used in the contemporary constructions. Among them King post truss, Queen post truss, Pratt truss, Fink truss, Howe truss, Fan truss, Fan Fink truss and Baltimore truss are most common for the pitched roof construction.

## 2.2. Self-similarity features of traditional trusses

From a geometric point of view, when the internal configuration of a truss is designed by assembling the posts, diagonals and struts within the main frame, the foremost target is always structural, dealing with the compressions and tensions in the members to obtain the maximum stability and high stiffness, and in some cases, it considers the aesthetic appearances too. While

the geometric constructions of the internal lattices of conventional trusses basically follows simple geometric rules, one striking feature, clearly recognizable in many examples, is the modular arrangement and repetition of simple geometric shapes at different scales. This repetition is meant for increasing the stiffness of the truss structure, by reducing the members slenderness. Generally, the more the repetitions are nested inside the truss frame, the more is the stiffness of the truss structure. In the ‘Figure 3’, it can be noticed that Double Howe truss, Fink truss and Fan Fink truss show some extend of self-similarity features at increasing orders of their compound configurations. In this figure, ‘A’ shape (King Post truss) is exactly or approximately copied in the second order configurations of Double Howe truss, Fink truss and Fan Fink truss with different orientations at different positions after its contraction. Similarly, ‘B’ shape (Fan truss) is also copied in the third order configuration of the Fan Fink truss. The geometric process of forming the compound configurations of these three conventional trusses derived from the very basic truss shapes such as King Post truss and Fan truss, illustrated in the ‘Figure 3’, somehow resembles with the rule-based process that generates self-similar

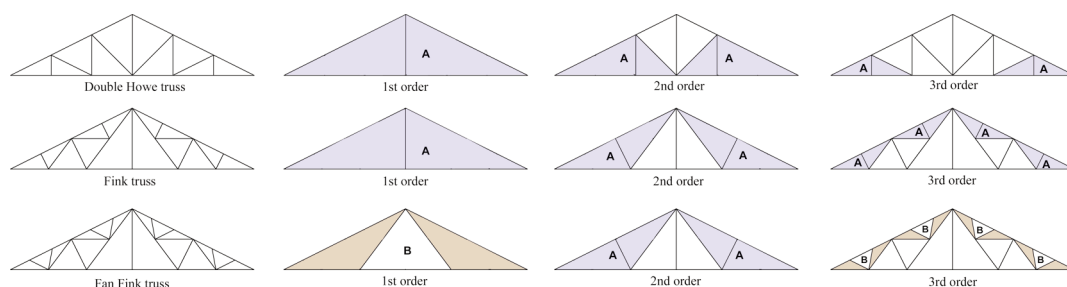


Figure 3. Some common types of trusses and their ‘self-similar’ features that are formed by the self-similar or self-affine repetitions of ‘A’ and ‘B’.

fractal shapes. Unaware with the notion of fractal geometry much before its introduction in 1970s by Mandelbrot, the engineers purposely used self-similar modular units to stiffen the conventional trusses. Accordingly, it is explorable to design rule-based self-similar features in the compound configurations of structural trusses that follow the principle of fractal geometry, and analyze the mechanical properties of these new fractal-based trusses.

### 3. FRACTAL GEOMETRY

#### 3.1. Mathematical characteristics of fractal geometry

A non-strict definition of a fractal is a shape or an image that contains the copies of itself at infinitely different range of scales; which means it is self-similar at every magnifying level. However, its mathematical definition is more precise. According to Robert L. Devany's (1992) mathematical definition, a fractal is a subset of  $R_n$  (an  $n$ -dimensional metric space) which is self-similar and whose Hausdorff dimension exceeds its topological dimension. In simpler description, fractal shapes are fractional dimensional and fall in between two successive integer dimensional objects, i.e.,  $0 < F_D < 1$ , or  $1 < F_D < 2$ , or  $2 < F_D < 3$ , where  $F_D$  is a fractal dimension. A fractal is a set which is a union of self-similar sets that lie in the Metric space, more precisely, in the Hausdorff Metric space. Based on the *contraction mapping theory* introduced by M. F. Barnsley (1988), a fractal set is an *attractor* when it is the resulting figure at the limit state obtained from a set of affine transformations ' $f_i$ ',  $i = 1$  to  $k$ , applied infinite times. An example, with just one transformation ' $f$ ', ( $k = 1$ ) is shown in 'Figure 4'.

A fractal is a unique non-empty compact set. The resulting figure can be obtained either by the *union* of all identical subsets or by the *intersection* of self-similar subsets.

When a fractal is an *attractor* ' $\Delta$ ' which is a *union* set of all the identical infinite subsets that are the scaled copies of initial set, then it is represented as,

$$\Delta = \bigcup_{n=0}^{\infty} \Delta_n \quad (3.1.1)$$

$$\text{i.e.,} \quad \Delta = \Delta_1 \cup \Delta_2 \cup \Delta_3 \cup \dots \cup \Delta_n \cup \Delta_0$$

$$\text{where,} \quad \Delta_n = \bigcup_{i=1}^m f_i(\Delta_{n-1}) \cup \Delta_0 \quad (3.1.2)$$

$$\Delta_1 = f_1(\Delta_0) \cup f_2(\Delta_0) \cup \dots \cup f_m(\Delta_0) \cup \Delta_0$$

$$\Delta_2 = f_1(\Delta_1) \cup f_2(\Delta_1) \cup \dots \cup f_m(\Delta_1) \cup \Delta_0$$

$$\Delta_n = f_1(\Delta_{n-1}) \cup f_2(\Delta_{n-1}) \cup \dots \cup f_m(\Delta_{n-1}) \cup \Delta_0$$

where,  $n$  is the number iterations and  $m$  is the number of self-similar copies produced at each iteration. When  $\Delta_1, \Delta_2, \dots, \Delta_n, \dots$  are contraction sets of  $\Delta_0$ , that are contracted by using the *contractivity factor*  $\lambda_i$  and transformed by using an *affine transformation* function  $f_i$ , such that,

$$\Delta_0 \subset \Delta_1 \subset \Delta_2 \subset \dots \subset \Delta_{n-1} \subset \Delta_n \subset \dots \quad (3.1.3)$$

then, they form a perfect self-similar fractal set.

When a fractal, as an *attractor*, is an *intersection* set of all the identical subsets of ' $K_0$ ', as shown in 'Figure 2', then the *attractor* ' $K$ ' can be expressed as,

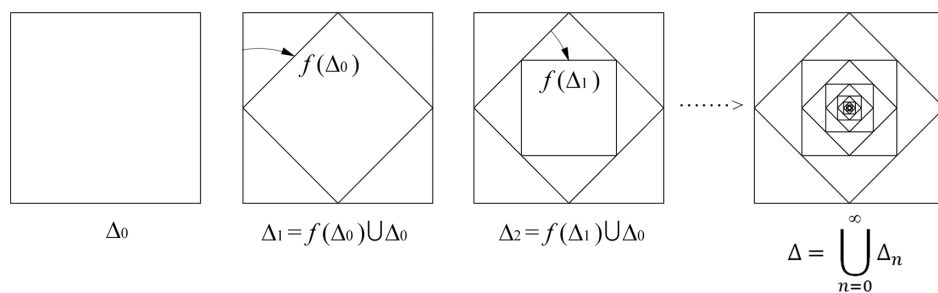


Figure 4. Fractal as a union of perfectly self-similar subsets after *affine transformation*.

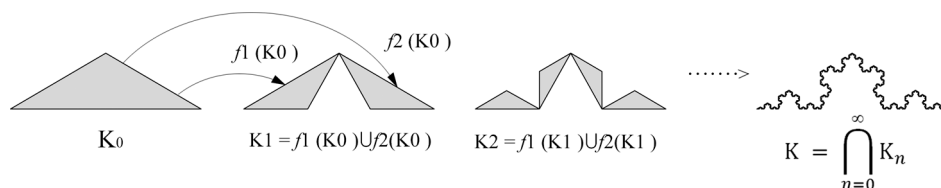


Figure 5. Fractal Koch curve, as an attractor which is an intersection of all perfectly self-similar subsets of ' $K_0$ ' after *affine transformations* of  $f_1$  and  $f_2$ .

$$K = \bigcap_{n=0}^{\infty} K_n \quad (3.1.4)$$

$$\text{i.e., } K = K_0 \cap K_1 \cap K_2 \cap K_3 \cap \dots \cap K_n \cap \dots$$

$$\text{where, } K_n = \bigcup_{i=1}^m f_i(K_{n-1}) \quad (3.1.5)$$

$$K_1 = f_1(K_0) \cup f_2(K_0) \cup \dots \cup f_m(K_0)$$

$$K_2 = f_1(K_1) \cup f_2(K_1) \cup \dots \cup f_m(K_1)$$

$$K_n = f_1(K_{n-1}) \cup f_2(K_{n-1}) \cup \dots \cup f_m(K_{n-1})$$

Again, if  $K_1, K_2, \dots, K_n, \dots$  are contraction sets of  $K_0$ , that are contracted by using the *contractivity factor*  $\lambda_i$  and transformed by using an *affine transformation function*  $f_i$ , such that,

$$K_0 \supset K_1 \supset K_2 \supset \dots \supset K_{n-1} \supset K_n \supset \dots \quad (3.1.6)$$

then, they form a perfect self-similar fractal set.

### 3.2. Iterated Function System (IFS)

Fractals are formed by the repetition of the original shape after the geometric transformations in the first step, and then repeating this process iteratively in the next steps for infinite times. This process leads to produce a fractal figure, which is, in many cases, unpredictable. However, in 1981, based on the Hutchinson's operator (Hutchinson, 1981), Barnsley developed a system, known as the *Iterated Function System* (IFS) that can predict the end result of a fractal formation in a deterministic way (Barnsley, 1988). In the Barnsley's concept of IFS, it is importantly noticed that the final outcome of the fractal figure is not defined by the initial shape. Instead, it is defined by *affine transformations* that can be regarded as the true 'initial condition'. In 'Figure 6', it is shown that a triangle and a hut shape separately converge into a Sierpinski triangle after a few iterations after keeping the *affine transformation rules* same for both the initial shapes.

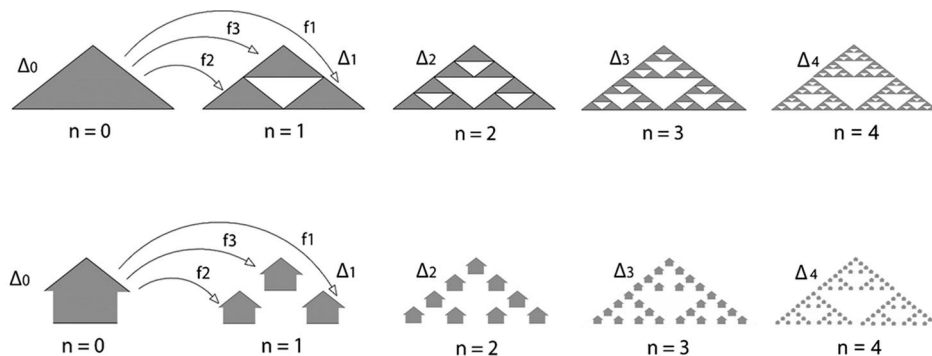


Figure 6. Convergent sequence of the Sierpinski triangle by using contraction mapping and IFS.  
Top: Initial shape is a triangle; Bottom – Initial shape is a hut.

Barnsley's *Iterated Function System* (IFS) is a simple but powerful function system that produces fractal figures in a deterministic way. It is shown in the 'Figure 6' that the main key operator of the IFS is a set of *affine transformations* that lead the final outcome towards an *attractor 'A'*. The IFS works recursively using the *Hutchinson operator* as shown in the 'Figure 7' to construct a self-similar fractal.

The figure resulted at the finite number of iterations ( $n$ ) is,

$$A_n = \bigcup_{i=1}^m f_i(A_{n-1}) \quad (3.2.1)$$

Therefore, from the properties of IFS, we notice the importance of *affine transformations* ' $f_i$ ' which is in fact the main key determinant for the *attractor 'A'*. The *affine transformation* ' $f$ ' can be expressed as,

$$f = T(x) + b \quad (3.2.2)$$

where, ' $T$ ' is a linear transformation (represented by a ' $n \times n$ ' matrix) and ' $b$ ' is a vector. The standard matrix form of the two-dimensional *affine transformation* in the Euclidean XY plane is represented as,

$$f(x) = [W]\{x\} + \{\delta\} = \begin{bmatrix} w_{11} & w_{12} \\ w_{21} & w_{22} \end{bmatrix} \begin{bmatrix} x \\ y \end{bmatrix} + \begin{bmatrix} \delta_x \\ \delta_y \end{bmatrix} \quad (3.2.3)$$

If the transformation consists of contraction, reflection, rotation and displacement, then 2.2.3 can be rewritten as:

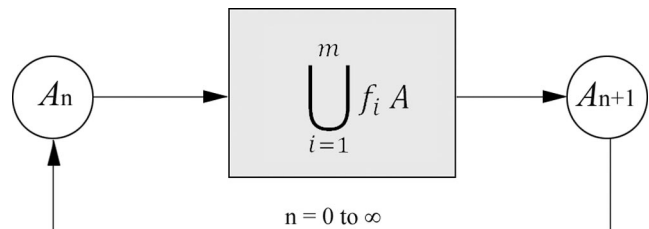


Figure 7. A schematic diagram that shows how IFS recursively calls output as input iteratively using the function of *Hutchinson operator*.



$$f = \lambda[\mu][r]\{x\} + \{\delta\}$$

$$= \lambda \begin{bmatrix} \mu_1 & 0 \\ 0 & \mu_2 \end{bmatrix} \begin{bmatrix} \cos \theta & -\sin \theta \\ \sin \theta & \cos \theta \end{bmatrix} \begin{bmatrix} x \\ y \end{bmatrix} + \begin{bmatrix} \delta_x \\ \delta_y \end{bmatrix} \quad (3.2.4)$$

where  $\mu_1 = -1$  and  $\mu_2 = 1$  is the reflections along Y-axis,  $\mu_1 = 1$  and  $\mu_2 = -1$  is the reflections along X-axis,  $\theta$  is the angle of rotation, and  $\delta_x$  and  $\delta_y$  are the displacement along X-axis and Y-axis respectively.

### 3.3. Hausdorff dimension

Hausdorff dimension is a mathematical measure that is mostly popular for evaluating the fractal dimension of self-similar fractals. Based on the Barnsley's *contraction mapping* theory (1988), the Hausdorff dimension of a fractal is linked to the *contractivity* factors by the following relation:

$$\sum_{i=1}^k \lambda_i^D = 1 \quad (3.3.1)$$

where  $\lambda_i$  is a *contractivity* factor of transformation  $f_i$  and  $k$  is the number of transformations.

For example, the Koch curve shown in 'Figure 5' is a union of two copies of itself, each copy shrunk by a factor  $1/\sqrt{3}$ . Its Hausdorff dimension  $D$  can be calculated by following way by using equation (3.3.1),

$$\sum_{i=1}^2 \left( \frac{1}{\sqrt{3}} \right)^D = 1$$

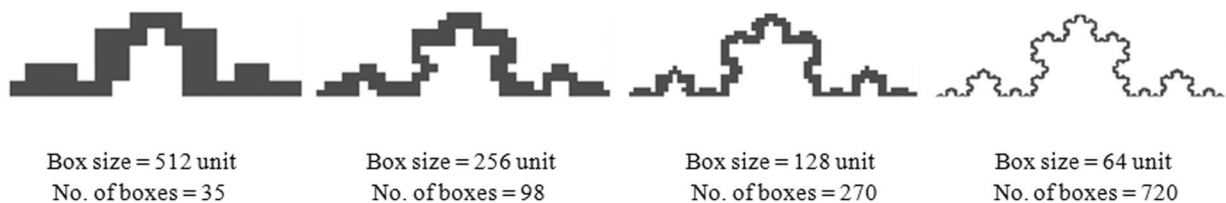
$$\text{i.e.,} \quad \left( \frac{1}{\sqrt{3}} \right)^D + \left( \frac{1}{\sqrt{3}} \right)^D = 2 \cdot \left( \frac{1}{\sqrt{3}} \right)^D = 1$$

$$\text{Therefore} \quad D = \frac{\log(1/2)}{\log(1/\sqrt{3})} \approx 1.262 \quad (3.3.2)$$

### 3.4. Box counting dimension

The Box Counting dimension, also known as Minkowski–Bouligand dimension, is another measure for estimating fractal dimension. While, Hausdorff method is suitable for calculating the fractal dimension of perfectly self-similar fractal shapes, the Box Counting dimension is useful for both self-similar and non-self-similar fractal shapes including any (mathematically) nonfractal figures, and importantly for finite shapes. This method is popular in analyzing the roughness or detailness of an image.

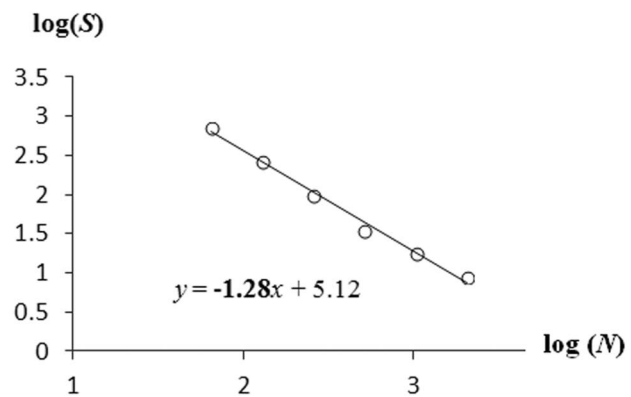
To evaluate the Box Counting dimension of an image, firstly a squares grid is overlaid on the image where the size of each grid box, let  $S$ , determines the scale of the grid. Then the boxes which cover any part



(a)

$S$	$N$	$\log(S)$	$\log(N)$
2048	9	3.31	0.95
1024	18	3.01	1.26
512	35	2.71	1.55
256	98	2.41	1.99
128	270	2.11	2.43
64	720	1.81	2.86

(b)



(c)

Figure 8. Calculation of Box Counting dimension of Koch curve using the 'Fractalyse' program. (a) Boxes that cover the any part Koch curve; (b) Number of covered boxes having with respect to different sizes; (c) Log-log graph that shows the slope of resulting line is 1.28, i.e. the Box Counting dimension of Koch curve is 1.28.

of the image within the grid, are counted; let it is  $N$ . After repeating the same process on the same image by changing the box size from 1 to  $2^n$  ( $n = 1, 2, 3, 4, \dots$ , finite value) fractal dimension  $D$  of that image can be obtained by transforming the results of  $S$  and  $N$  into the log-log graph. The slope of the resulting line of the log-log graph determines the *Box Counting dimension* of the image. One example has been demonstrated in the 'Figure 8' to calculate the fractal dimension of Koch curve by using the Box Counting method. It is important to mention that the fractal dimensions measured by using Hausdorff method and Box Counting method not necessarily provide exactly the same value, but near value. For example, in the case of Koch curve, the Hausdorff dimension is nearly 1.262 and the Box Counting dimension is 1.28.

#### 4. MODELING OF FRACTALS AND THEIR DIMENSIONS

Fractal system has two important properties that are useful for structural design in the field of construction. The first property is that the fractal system can be expressed by using a simple algorithmic function. This property is useful for easily programming a fractal model in computer for designing structures. Second, fractal system is an assembly of some self-similar unit elements; hence, they form some hierarchical or modular system in structure. This property can be useful to construct long-span structures where modular units are required for stiffening and strengthening a structure. There are different methods to design a simple algorithmic function that can generate a fractal model. In this paper, Barnsley's method (1988) of fractal construction is adopted which is based on his *contraction mapping* theorem and the Iterated Function System. Using his method and the principle of fractal geometry, some fractal models are constructed in this study in order to make different geometric configurations of some structural trusses. First two trusses are designed based on the well-known fractals such as Sierpinski triangle and Pinwheel Fractal, whereas other trusses are designed by reorganizing the configurations of traditional trusses using fractal rule. Asayama and Mae's (2004) fractal truss is also included in this family of fractal-based trusses.

##### 4.1. Sierpinski triangle

Sierpinski triangle is a canonical example of fractal geometry. By its construction, generally, a triangle ' $S_0$ ', as an initiator, is subdivided into four identical

triangles and then the central sub-triangle is discarded. This process continues to the other remaining three sub-triangles to produce further smaller congruent sub-triangles, and thus continue this process on each remaining smaller sub-triangles ad infinitum. Sierpinski triangle can be generated by using Barnsley's *Iterated Function System* (IFS) method based on his theory of *contraction mappings* and *affine transformations*. In this method, Sierpinski triangle ' $S$ ' is an *attractor* which is an intersection set of all the infinitely iterated self-similar sets that are ' $S_0$ ', ' $S_1$ ', ' $S_2$ ', ' $S_3$ ',  $\dots$ , ' $S_n$ ',  $\dots$ . In this method of constructing a Sierpinski triangle, the IFS produces three identical copies (' $\sigma_1$ ', ' $\sigma_2$ ' and ' $\sigma_3$ ') from initial triangle ' $S_0$ ' at the first iteration using the *contractivity* factor  $\lambda$  as 1/2 and the *affine transformation* functions as  $f_i$ , shown in 'Figure 9'. Thus, a new shape ' $S_1$ ' is generated which is a union of ' $\sigma_1$ ', ' $\sigma_2$ ' and ' $\sigma_3$ ', mathematically expressed as,

$$S_1 = \sigma_1 \cup \sigma_2 \cup \sigma_3 = f_1(S_0) \cup f_2(S_0) \cup f_3(S_0) \quad (4.1.1)$$

At  $n_{th}$  iteration

$$S_n = f_1(S_{n-1}) \cup f_2(S_{n-1}) \cup f_3(S_{n-1}) \quad (4.1.2)$$

$$\text{such that } S_0 \supset S_1 \supset S_2 \supset S_3 \supset \dots \supset S_{n-1} \supset S_n \supset \dots \quad (4.1.3)$$

Hence, the attractor ' $S$ ' is,

$$S = \bigcap_{i=1}^{\infty} S_i \quad (4.1.4)$$

which is a mathematical expression of Sierpinski triangle, a fractal entity.

In the case of constructing the Sierpinski triangle, the following function of IFS is applied that consists of  $k = 3$  different *affine transformations* ( $f_1, f_2$  and  $f_3$ ) of the original triangle shown in 'Figure 9'.

$$f_i = \lambda_i \begin{bmatrix} \mu_1 & 0 \\ 0 & \mu_2 \end{bmatrix} \begin{bmatrix} \cos \theta & -\sin \theta \\ \sin \theta & \cos \theta \end{bmatrix} \begin{bmatrix} x \\ y \end{bmatrix} + \begin{bmatrix} \delta_x \\ \delta_y \end{bmatrix}; i = 1 \text{ to } 3 \quad (4.1.5)$$

Based on the equation (3.3.1), if the Hausdorff dimension of Sierpinski triangle is  $D$ , then

$$\lambda_1^D + \lambda_2^D + \lambda_3^D = 1; \quad \text{where, } \lambda_1 = \lambda_2 = \lambda_3 = \frac{1}{2} \quad (4.1.6)$$

$$\text{Therefore, } \left(\frac{1}{2}\right)^D + \left(\frac{1}{2}\right)^D + \left(\frac{1}{2}\right)^D = 3 \cdot \left(\frac{1}{2}\right)^D = 1 \quad (4.1.7)$$

$$\text{So, } D = \frac{\log(1/3)}{\log(1/2)} \approx 1.585$$

IFS functions	Contractivity	Reflection		Rotation	Displacement	
$f$	$\lambda$	$\mu_1$	$\mu_2$	$\theta$	$\delta_x$	$\delta_y$
$f_1$	$\frac{1}{2}$	1	1	$0^\circ$	0	0
$f_2$	$\frac{1}{2}$	1	1	$0^\circ$	$2L$	0
$f_3$	$\frac{1}{2}$	1	1	$0^\circ$	$L$	$L/2$

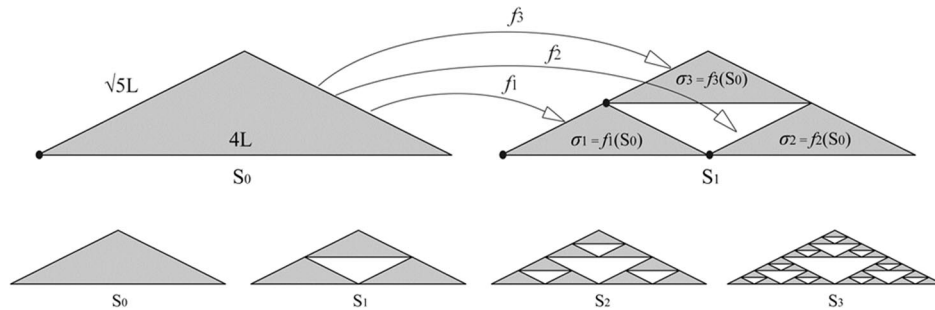


Figure 9. Top - Contraction mapping and affine transformation of the Sierpinski triangle. Contractivity is  $1/2$ ;  
Bottom – Convergent sequence of Sierpinski triangle.

## 4.2. Pinwheel fractal

### 4.2.1. Pinwheel tiling

An interesting opportunity to create fractal shapes is given by a non periodic tiling of the plane, as the well known Pinwheel Tiling developed by John Conway and Charles Radin in 1994 (Radin and Conway, 1995). Pinwheel Tiling is an assembly of identical triangular tiles yet produces randomness with high visual complexity. It is a non-periodic tiling which means their orientations is infinite and do not follow the same orientations. Conway, first noticed that a right-angled triangle ' $P_0$ ' having its width double than its height can be divided in five isometric copies of itself that are ' $t$ 's, where each copy is  $1/\sqrt{5}$  times smaller than ' $P_0$ '. Starting from that, Conway and Radin assembled four copies of the triangle ' $P_0$ ' around it such a way so that the union of five isometric triangles becomes a big

right-angled triangle ' $P_1$ ' (Figure 10). Now, around the ' $P_1$ ', its four isometric copies are translated and assembled in the similar fashion so that the union of all triangles of ' $P_1$ ' and its copies becomes a larger triangle ' $P_2$ '. This process can be iterated to obtain an infinite increasing sequence of growing triangles where all the new triangular planes are the isometric copies of ' $P_0$ '. In this tiling, one interesting feature appears is the infinitely many orientations of the tiles. This is because of the two angles of the ' $P_0$ ' which are  $\arctan(1/2)$  and  $\arctan(2)$ , and both of these values are both non-commensurable with  $\pi$ . Despite this, Radin and Conway (1995) confirm that all the vertices of the isometric copies of ' $P_0$ ' in the tiling have rational coordinates. In this sense, Pinwheel Tiling is not exactly repetitive.

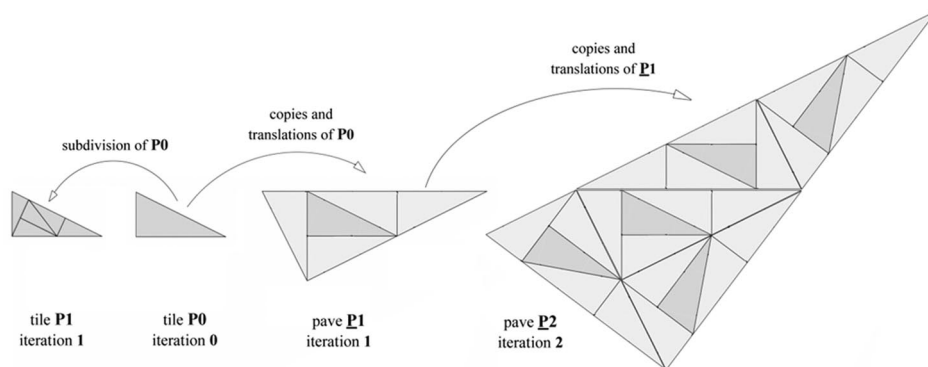


Figure 10. Conway and Radin's method to make Pinwheel tiling pattern which starts from one small triangle tile and then it iteratively grows outwards with above rule.

The pinwheel tiling can even be regarded as an iterated subdivision of an initial shape ' $P_0$ ', so that the generating procedure becomes similar to the iterated function system. In this context, Barnsley's method can be applied. In this case, ' $P_0$ ' is an initial triangle and it will be subdivided to produce pinwheel tiling pattern. Using, the *contraction mapping* process on the main triangle ' $P_0$ ', five isometric copies ( $t_1, t_2, t_3, t_4$  and  $t_5$ ) are generated which are *contraction mappings* of ' $P_0$ ' itself using the *contractivity* factor of  $1/\sqrt{5}$ . Then, each of them pass through a unique *affine transformation* process so that all of them can converge into and accommodated inside the space of main triangle ' $P_0$ ' without overlapping but touching with each other (Figure 11, above).

The output figure at the first iteration can be expressed as,

$$P_1 = t_1 \cup t_2 \cup t_3 \cup t_4 \cup t_5 \\ = f_1(P_0) \cup f_2(P_0) \cup f_3(P_0) \cup f_4(P_0) \cup f_5(P_0) \quad (4.2.1)$$

and at  $n$ th iteration, 
$$P_n = \bigcup_{i=1}^5 f_i(P_{n-1}) \quad (4.2.2)$$

$$\text{where, } P_0 \supset P_1 \supset P_2 \supset P_3 \supset \dots \supset P_{n-1} \supset P_n \supset \dots \quad (4.2.3)$$

Hence, the Pinwheel Tiling as an *attractor* ' $C$ ' is an intersection set of all the identical subsets of ' $P_0$ ', and can be expressed as,

$$C = \bigcap_{i=1}^{\infty} P_i \quad (4.2.4)$$

In the case of constructing the Pinwheel Tiling, the following function of IFS is applied that consists  $k = 5$  different *affine transformations* (' $f_1$ ', ' $f_2$ ', ' $f_3$ ', ' $f_4$ ' and ' $f_5$ ') of the main triangle.

$$f_i = \lambda_i \begin{bmatrix} \mu_1 & 0 \\ 0 & \mu_2 \end{bmatrix} \begin{bmatrix} \cos \theta & -\sin \theta \\ \sin \theta & \cos \theta \end{bmatrix} \begin{bmatrix} x \\ y \end{bmatrix} + \begin{bmatrix} \delta_x \\ \delta_y \end{bmatrix}; i = 1 \text{ to } 5 \quad (4.2.5)$$

According to the Hausdorff dimension method, if the fractal dimension of a Pinwheel Tiling is  $D$ , then

$$\lambda_1^D + \lambda_2^D + \lambda_3^D + \lambda_4^D + \lambda_5^D = 1 \quad (4.2.6)$$

IFS functions	Contractivity	Reflection		Rotation	Displacement	
$f$	$\lambda$	$\mu_1$	$\mu_2$	$\theta$	$\delta_x$	$\delta_y$
$f_1$	$1/\sqrt{5}$	-1	1	$-(90^\circ + \arctan(1/2))$	0.2L	0.4L
$f_2$	$1/\sqrt{5}$	-1	1	$-\arctan(2)$	0.4L	0.8L
$f_3$	$1/\sqrt{5}$	1	1	$-(90^\circ + \arctan(1/2))$	1.2L	0.4L
$f_4$	$1/\sqrt{5}$	-1	1	$-(90^\circ + \arctan(1/2))$	1.2L	0.4L
$f_5$	$1/\sqrt{5}$	1	1	$\arctan(1/2)$	0.2L	0.4L

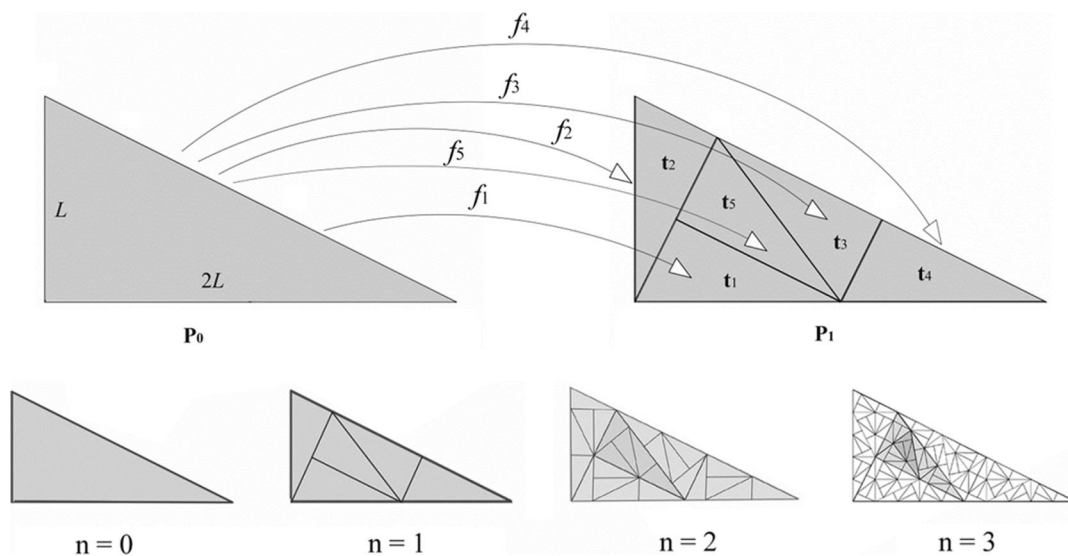


Figure 11. Pinwheel Tiling construction using *contraction mapping* method; Above - Affine transformations of right-angle triangle. Bottom - Convergent sequence of Pinwheel Tiling.

where  $\lambda_1 = \lambda_2 = \lambda_3 = \lambda_4 = \lambda_5 = \frac{1}{\sqrt{5}}$

Hence,  $5 \cdot \left( \frac{1}{\sqrt{5}} \right)^D = 1$

i.e.,  $D = \frac{\log(1/5)}{\log(1/\sqrt{5})} = 2$  (4.2.7)

The calculated Hausdorff dimension of this iterated figure of Pinwheel Tiling is 2 which is an integer value, and it is equivalent to a two dimensional surface. That is obvious in the subdivision (or tiling) process, because no surface is added or subtracted at each iteration.

#### 4.2.2. Pinwheel fractal

If the central triangle of Pinwheel Tiling is discarded ad infinitum, then the whole triangular surface starts losing its dimension (Hausdorff dimension,  $D$ ) from 2 to fractional such that  $1.0 < D < 2.0$ . Thus, it becomes no longer a two dimensional surface and transforms into a fractal shape, which is known as a Pinwheel Fractal (Figure 12). So, in this situation, the Pinwheel Fractal as an attractor ' $P$ ', which is an intersection set of all the identical subsets of ' $P_0$ ', can be expressed as,

$$P = \bigcap_{i=1}^{\infty} P_i \quad (4.2.8)$$

where,

$$P_1 = t_1 \cup t_2 \cup t_3 \cup t_4 = f_1(P_0) \cup f_2(P_0) \cup f_3(P_0) \cup f_4(P_0) \quad (4.2.9)$$

$$\text{and} \quad P_n = \bigcup_{i=1}^4 f_i(P_{n-1}) \quad (4.2.10)$$

Hence,

$$P_n = f_1(P_{n-1}) \cup f_2(P_{n-1}) \cup f_3(P_{n-1}) \cup f_4(P_{n-1}) \quad (4.2.11)$$

If the Hausdorff dimension of Pinwheel Fractal is  $D$ , then

$$4 \cdot \left( \frac{1}{\sqrt{5}} \right)^D = 1$$

$$\text{Hence,} \quad D = \frac{\log(1/4)}{\log(1/\sqrt{5})} \approx 1.7227 \quad (4.2.12)$$

#### 4.3. Asayama and Mae's fractal

Asayama and Mae (2004) were the first who proposed a new fractal shape for designing a truss by using IFS method. The first iterated figure of their fractal was formed by the union of three self-similar copies (' $\alpha_1$ ', ' $\alpha_2$ ' and ' $\alpha_3$ ') of the first triangle ' $\Delta_0$ ' after its two dimensional *affine transformations* ( $f_1, f_2$  and  $f_3$ ) in which the contractions are  $\lambda_1, \lambda_2$  and  $\lambda_3$  (Figure 13). In their design, the initial triangle ' $\Delta_0$ ' is a parametric and variable to the base angles  $\theta_1$  and  $\theta_2$ , and accordingly the *contractivities* of their fractal are variable to the base angles. However, in our study, we have taken the symmetric triangle with the height  $L$  and base  $4L$  so that the contractions are  $\lambda_1 = \sqrt{5}/4$ ,  $\lambda_2 = \sqrt{5}/4$  and  $\lambda_3 = 3/8$ . In this condition, the Asayama-Mae's fractal as an *attractor* ' $\Delta$ ' can be represented as,

$$\Delta = \bigcap_{i=1}^{\infty} \Delta_i$$

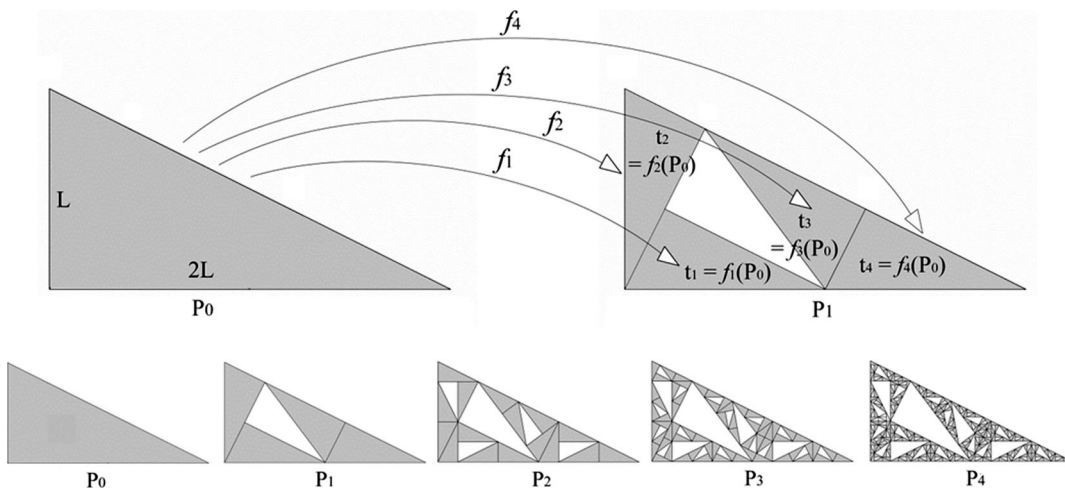


Figure 12. Pinwheel Fractal; Above - Affine transformations; Bottom – Convergent sequence.



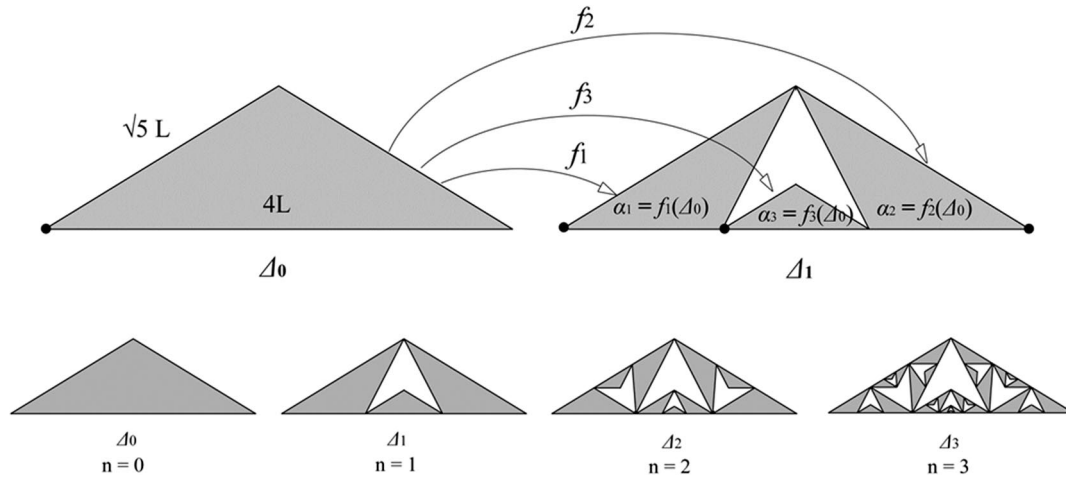


Figure 13. Asayama and Mae's Fractal; Above - Affine transformations; Bottom – Convergent sequence.

in which,

$$\Delta_1 = \alpha_1 \cup \alpha_2 \cup \alpha_3 = f_1(\Delta_0) \cup f_2(\Delta_0) \cup f_3(\Delta_0) \quad (4.3.1)$$

$$\text{and } \Delta_n = f_1(\Delta_{n-1}) \cup f_2(\Delta_{n-1}) \cup f_3(\Delta_{n-1}) \quad (4.3.2)$$

$$\text{where, } \Delta_0 \supset \Delta_1 \supset \Delta_2 \supset \Delta_3 \supset \dots \supset \Delta_{n-1} \supset \Delta_n \supset \dots \quad (4.3.3)$$

The *affine transformations* of this fractal shape can be expressed as follows,

$$f_i = \lambda_i \left[ \begin{array}{cc} \mu_1 & 0 \\ 0 & \mu_2 \end{array} \right] \left[ \begin{array}{cc} \cos \theta & -\sin \theta \\ \sin \theta & \cos \theta \end{array} \right] \left[ \begin{array}{c} x \\ y \end{array} \right] + \left[ \begin{array}{c} \delta_x \\ \delta_y \end{array} \right]; i = 1 \text{ to } 3 \quad (4.3.4)$$

Based on the equation (3.3.1), if the Hausdorff dimension of the Asayama-Mae's Fractal is  $D$ , then

$$\left( \frac{1}{\sqrt{5}} \right)^D + \left( \frac{1}{\sqrt{5}} \right)^D + \left( \frac{3}{8} \right)^D = 1 \quad (4.3.5)$$

Using the Newton-Raphson method, we get  $D \approx 1.5953$

The Hausdorff dimension of Asayama-Mae's Fractal is about 1.5953 when the base angles are the same which is  $\arctan(1/2)$ . But, in fact, the Hausdorff dimension of this fractal is variable to the base angles, because the contractions,  $\lambda_i = \text{function}(\theta_1, \theta_2)$ , as demonstrated by Asayama and Mae (2004).

#### 4.4. Fan fractal

Fan Fractal is also constructed by following the same process as above based on the IFS method. In this case, ' $F_0$ ' is the initial shape, and the  $n$ th iterated shape ' $F_n$ ' is the union of the two contracted shapes of their previous shape ' $F_{n-1}$ ' after the two affine transformations  $f_1$  and  $f_2$  shown in 'Figure 14'. In this figure, the dotted lines are shown as the impressions of previous shapes which will be used as a guide for designing its corresponding truss configuration in the next section. Here, the *contractivities* of two self-similar copies are equal which is  $\sqrt{5}/4$ . So, the Fan Fractal as an *attractor* ' $F$ ' is an *intersection* set of all the identical subsets of ' $F_0$ ', and can be expressed as,

$$F = \bigcap_{i=1}^{\infty} F_i \quad (4.4.1)$$

$$\text{in which } F_1 = \varphi_1 \cup \varphi_2 = f_1(F_0) \cup f_2(F_0) \quad (4.4.2)$$

$$\text{and } F_n = f_1(F_{n-1}) \cup f_2(F_{n-1}) \quad (4.4.3)$$

$$\text{where, } F_0 \supset F_1 \supset F_2 \supset F_3 \supset \dots \supset F_{n-1} \supset F_n \supset \dots \quad (4.4.4)$$

IFS functions	Contractivity	Reflection		Rotation	Displacement	
$f$	$\lambda$	$\mu_1$	$\mu_2$	$\theta$	$\delta_x$	$\delta_y$
$f_1$	$\sqrt{5}/4$	1	-1	$-\arctan(1/2)$	0	0
$f_2$	$\sqrt{5}/4$	1	1	$-2 \cdot \arctan(2)$	4L	0
$f_3$	3/8	1	1	0°	5L/4	0

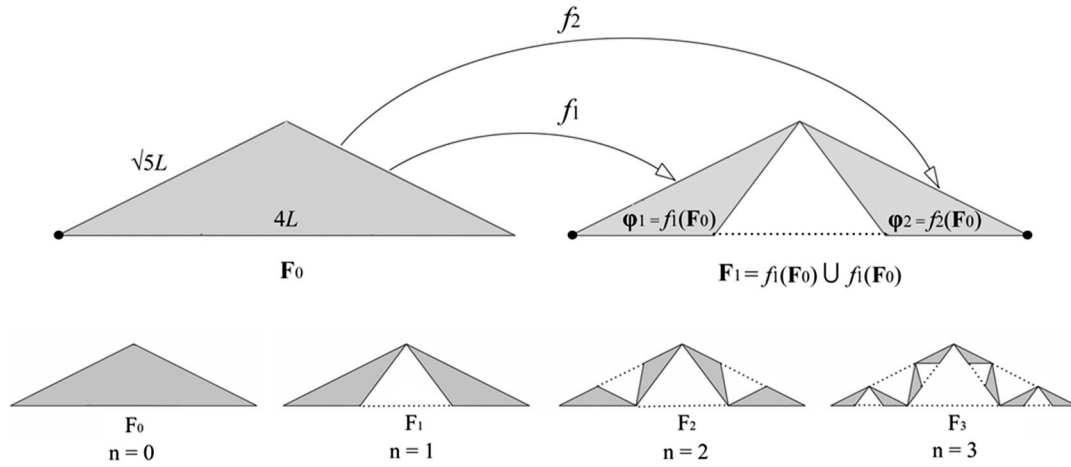


Figure 14. Fan Fractal; Above - Affine transformations; Bottom – Convergent sequence. (The dotted lines are the impressions of previous shapes.)

The two-dimensional *affine transformations* of the Fan Fractal shape in the Euclidean XY plane is,

$$f_i = \lambda_i \begin{bmatrix} \mu_1 & 0 \\ 0 & \mu_2 \end{bmatrix} \begin{bmatrix} \cos \theta & -\sin \theta \\ \sin \theta & \cos \theta \end{bmatrix} \begin{bmatrix} x \\ y \end{bmatrix} + \begin{bmatrix} \delta_x \\ \delta_y \end{bmatrix}; i = 1 \text{ to } 2 \quad (4.4.5)$$

If the Hausdorff dimension of a Fan Fractal shape is  $D$ , then

$$\left(\frac{\sqrt{5}}{4}\right)^D + \left(\frac{\sqrt{5}}{4}\right)^D = 2 \cdot \left(\frac{\sqrt{5}}{4}\right)^D = 1 \quad (4.4.6)$$

$$\text{Therefore, } D = \frac{\log(1/2)}{\log(\sqrt{5}/4)} \approx 1.1918 \quad (4.4.7)$$

#### 4.5. Baltimore fractal

Based on the similar method used for the constructions of previous fractals, the Baltimore Fractal is constructed by the union of the two contractions of previous shape at each new iteration using the *affine transformations*  $f_1$  and  $f_2$  (Figure 15). Unlike other fractals, the initial shape ' $B_0$ ' of the Baltimore Fractal is a triangle having an additional vertical line that connects the vertex to the middle of base line (Figure 15a). Similar as the construction of the Fan Fractal, the dotted lines shown in the 'Figure 15' are the impressions of previously iterated shape. The shape of Baltimore Fractal as an *attractor* ' $B$ ' and its corresponding *affine transformations* can be expressed as,

$$B = \bigcap_{i=1}^{\infty} B_i \quad (4.5.1)$$

$$\text{where, } B_1 = b_1 \cup b_2 = f_1(B_0) \cup f_2(B_0) \quad (4.5.2)$$

$$\text{i.e., } B_n = f_1(B_{n-1}) \cup f_2(B_{n-1}) \quad (4.5.3)$$

$$\text{so that, } B_0 \supset B_1 \supset B_2 \supset B_3 \supset \dots \supset B_{n-1} \supset B_n \supset \dots \quad (4.5.4)$$

Affine transformation,

$$f_i = \lambda_i \begin{bmatrix} \mu_1 & 0 \\ 0 & \mu_2 \end{bmatrix} + \begin{bmatrix} \cos \theta & -\sin \theta \\ \sin \theta & \cos \theta \end{bmatrix} \begin{bmatrix} x \\ y \end{bmatrix} + \begin{bmatrix} \delta_x \\ \delta_y \end{bmatrix}; i = 1 \text{ to } 2 \quad (4.5.5)$$

If the Hausdorff dimension of a Baltimore Fractal shape is  $D$ ,

$$\text{then, } \left(\frac{1}{2}\right)^D + \left(\frac{1}{2}\right)^D = 2 \cdot \left(\frac{1}{2}\right)^D = 1$$

$$\text{Therefore, } D = \frac{\log(2)}{\log(2)} = 1.00 \quad (4.5.6)$$

which means, at infinite iteration, the Baltimore Fractal (without dotted lines) will be transformed into a one dimensional line.

IFS functions	Contractivity	Reflection		Rotation	Displacement	
$f$	$\lambda$	$\mu_1$	$\mu_2$	$\theta$	$\delta_x$	$\delta_y$
$f_1$	$\sqrt{5}/4$	1	-1	$-\arctan(1/2)$	0	0
$f_2$	$\sqrt{5}/4$	1	1	$-2 \cdot \arctan(2)$	4L	0

IFS functions	Contractivity	Reflection		Rotation	Displacement	
$f$	$\lambda$	$\mu_1$	$\mu_2$	$\theta$	$\delta_x$	$\delta_y$
$f_1$	1/2	1	1	0°	0	0
$f_2$	1/2	1	1	0°	2L	0

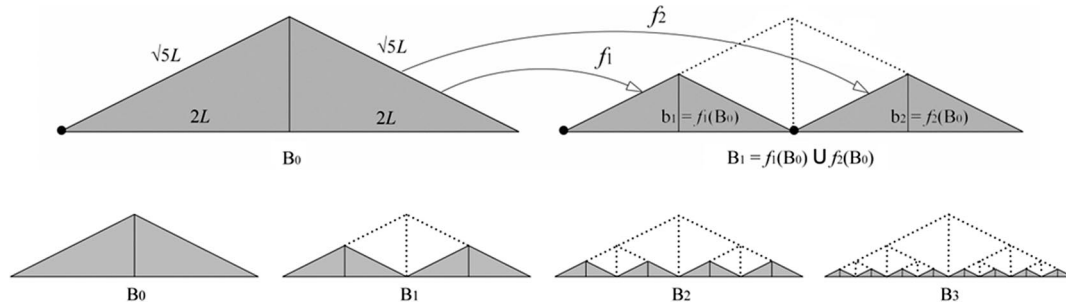


Figure 15. Top - Contraction mapping and affine transformation of the Baltimore Fractal Truss.  
Bottom – Convergent sequence of Baltimore Fractal Truss.

#### 4.6. Comparison of the Hausdorff dimensions

In the previous sections, the Hausdorff dimensions of all five fractal shapes are calculated by using Barnsley's *contraction mapping* method (1988) considering all the triangles have the same base angles  $\theta_1$  and  $\theta_2$  such a way so that  $\theta_1 = \theta_2 = \arctan(1/2)$ . It is observed that the estimated Hausdorff dimensions are variable to the base angles  $\theta_1$  and  $\theta_2$  in the case of Fan Fractal shape and Asayama-Mae's Fractal shape. Because, in these two shapes the contractions are related to the base angles. Oppositely, in the cases of Sierpinski triangle, Pinwheel Fractal shape and Baltimore Fractal shape, their contractions are not related to the base angles, and hence, the Hausdorff dimensions in these three fractal shapes are constant and invariable to the base angles. The comparative values of Hausdorff dimensions of these five fractal shapes are shown in 'Figure 16'.

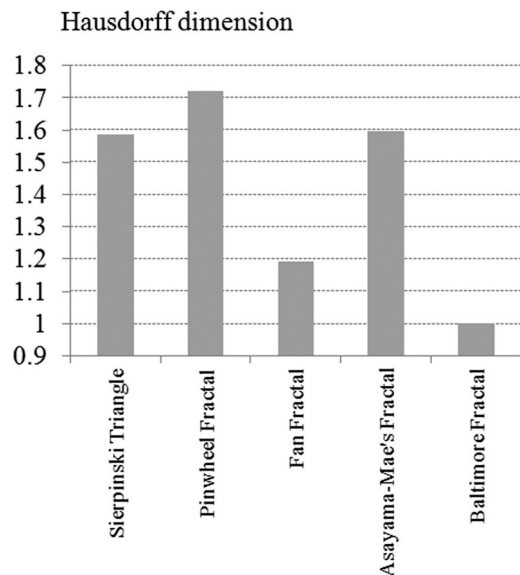


Figure 16. A comparison of the Hausdorff dimensions.

## 5. DESIGN OF FRACTAL-BASED TRUSSES

### 5.1. Design considerations and truss designs

Five different fractal shapes, which are constructed in the previous section using IFS method, are transformed into the geometric configurations useful for designing pitched roof trusses. A fractal is an infinite entity. Therefore, in the scale of architecture and engineering, only finitely iterated fractal models are applicable. The following considerations are taken into account for transforming the mathematical fractal shapes into the truss designs,

- Only the third iterated fractal models are considered as the truss configurations except the Pinwheel Fractal shape which is its second iterated model. These finitely iterated models are chosen by keeping the overall size of each truss in mind so that the longest member and the shortest member of the truss do not become too long and too short with respect to their cross-sections.
- The overall height of each truss is 3 meters; hence, the base is 12 meters wide, because it is considered in the beginning that the length of its

- base is always 4 times more than its height for each truss.
- Only the line segments (i.e., the outer lines of all shaded parts) of the above fractal shapes are considered for designing the truss lattices.
  - All the individual lines are considered as truss members and their connecting points as truss joints.
  - Each member is made of steel having a circular hollow cross-section with 6 cm diameter and 3 mm thickness.
  - Each joint is a steel plate which connects steel tubular members and acts as a hinged joint. The connecting system at the joints is made such a way so that the posts and diagonals, which are attached to the rafters and their junction, act as hanging members; and the other members, which are attached to the tie beam, carry the weight of tie beam (Figure 20b). This connecting system is followed by the similar mechanism as traditional King post truss shown in 'Figure 2a'.
  - Two far end joints at the base of each truss are considered as two supports. One support is

vertically and horizontally restrained, while another one is only vertically restrained as a roller.

Based on the above design considerations, the third iterated shapes of the Sierpinski triangle and the Asayama-Mae's Fractal are straightforwardly transformed into the designs of Sierpinski Fractal truss and Asayama-Mae's Fractal truss by only taking the outlines of their shaded parts (Figure 17). Two copies of the second iterated shapes of Pinwheel Fractal are attached by placing them opposite to each other along their heights, and then transform this jointed shape into the design of Pinwheel Fractal truss (Figure 17).

Fan Fractal and Baltimore Fractal shapes are also transformed into line lattices for designing their corresponding trusses, but by adding new line ' $F$ ' and a group of lines ' $B$ ' respectively at each new iteration such a way so that these new lines replaces of dotted lines that were shown in 'Figure 18' and 'Figure 19'. The intention is to obtain truss-like configurations. This new addition in Fan Fractal is marked as red lines and shown in 'Figure 18'. Now, this new shape ' $F_i$ ' can be expressed as follows:

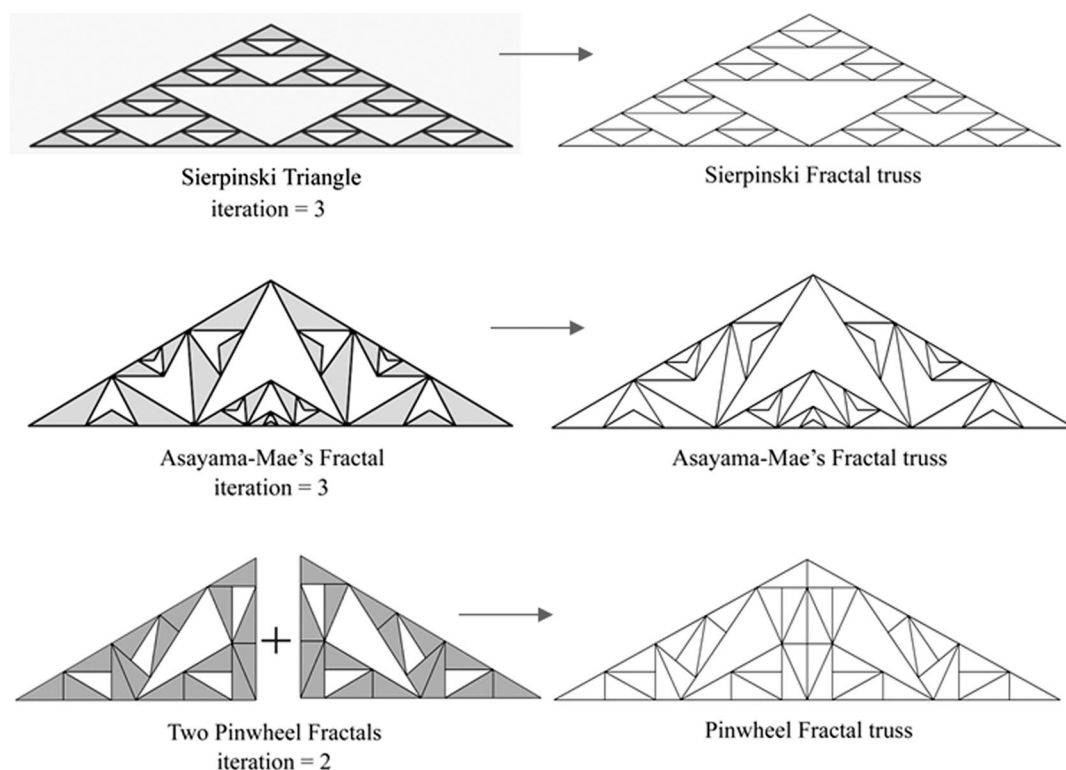


Figure 17. Fractal-based trusses design by transforming the the third iterated models of Sierpinski Triangle and Asayama-Mae's Fractal, and the second iterated model of Pinwheel Fractal.

$$F_t = \bigcap_{i=1}^{\infty} F_i \quad (5.1.1)$$

in which

$$F_1 = \varphi_1 \cup \varphi_2 \cup F = f_1(F_0) \cup f_2(F_0) \cup F; \quad F \subset F_t \quad (5.1.2)$$

$$\text{and} \quad F_n = f_1(F_{n-1}) \cup f_2(F_{n-1}) \cup F \quad (5.1.3)$$

Similarly, a group of new lines added in Baltimore Fractal is marked as red lines and shown in 'Figure 19'. The new shape ' $B_t$ ' of Baltimore Fractal, now, can be expressed as follows:

$$B_t = \bigcap_{i=1}^{\infty} B_i \quad (5.1.4)$$

where

$$B_1 = b_1 \cup b_2 \cup B = f_1(B_0) \cup f_2(B_0) \cup B; \quad B \subset B_t \quad (5.1.5)$$

$$\text{i.e.,} \quad B_n = f_1(B_{n-1}) \cup f_2(B_{n-1}) \cup B \quad (5.1.6)$$

In the 'Figure 21, left', we have calculated the Box Counting dimension of each line lattice to measure its density inside the main triangular frame. Apparently, the denser the internal lattice of a truss, the stiffer is the truss structure having a reasonable topology. The comparative values of Box Counting dimensions are shown in 'Figure 21, left' which informs the degree of lattice density among all five fractal-based trusses. It will be interesting to see if there is some relations between the Box Counting dimension and the stiffness of a truss.

Based on the above design considerations, we calculated the total weights of all truss structures, and their comparison is shown in 'Figure 21, right'. It is seen that there is a similarity between Box Counting dimension differences of the trusses and their weight differences. This is understandable, because, the denser the lattice, the heavier is the truss. In this sense, Box Counting dimension can be interpreted as visual measure of truss weights.

## 5.2. Statical determinacy of fractal-based trusses

For the practical applicability of the fractal-based new trusses in construction, it is important to check if they are statically determinate or not as a measure of their internal stabilities. Generally, this property of a truss is checked based on the rule of force equilibrium in which the total number of unknown forces  $F$  and the total numbers of equilibrium equations  $E_q$  are counted and compared. If,  $F < E_q$ , then the truss is a hypostatic, i.e., statically indeterminate; if,  $F = E_q$ , then the truss is an isostatic, i.e., statically determinate; and if  $F > E_q$ , then the truss is a hyperstatic, i.e., statically indeterminate. It is evaluated in 'Table 1' that informs whether the fractal-based trusses are statically determinate or indeterminate.

From the 'Table 1', we notice that all the fractal-based trusses are statically determinate, except Pinwheel Fractal truss. To transform the Pinwheel Fractal truss into an isostatic truss, some members should be eliminated such a way so that  $F = E_q$ . So, the number of eliminated members should be  $= F - E_q = (2b - 2j + r) = (81 - 2 \times 40 + 3) = 4$  without

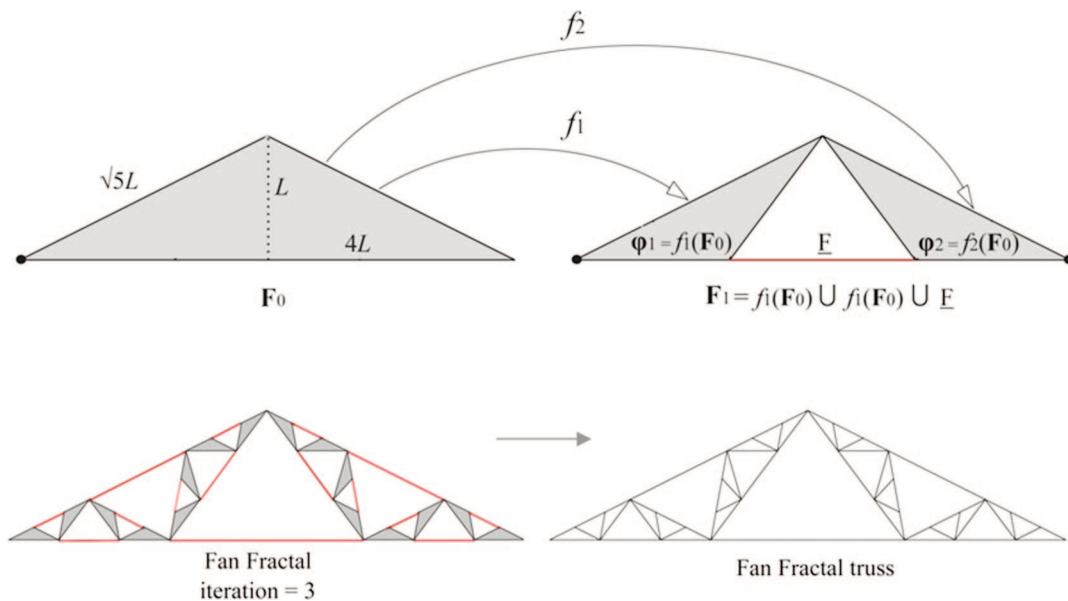


Figure 18. Transformation of third iterated Fan Fractal into its corresponding truss design by adding a newline  $F$  at each iteration.



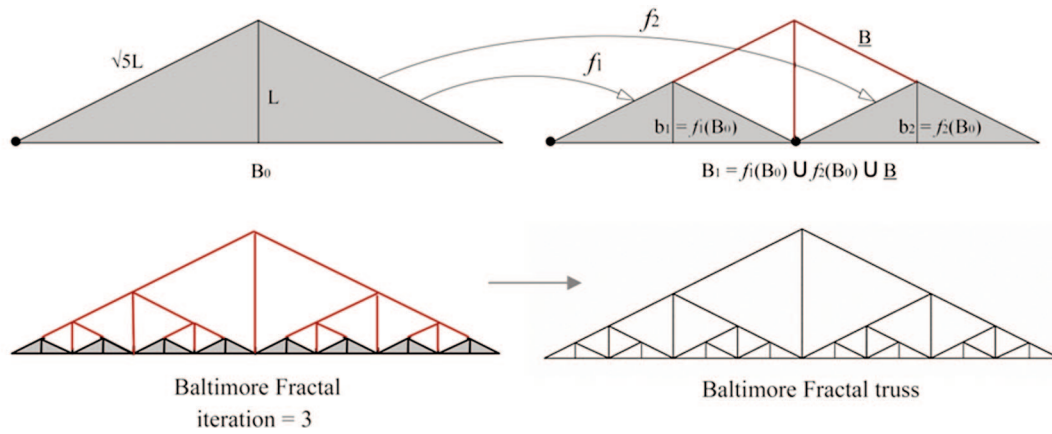


Figure 19. Transformation of third iterated Baltimore Fractal into its corresponding truss design by adding a new line  $B$  at each iteration.

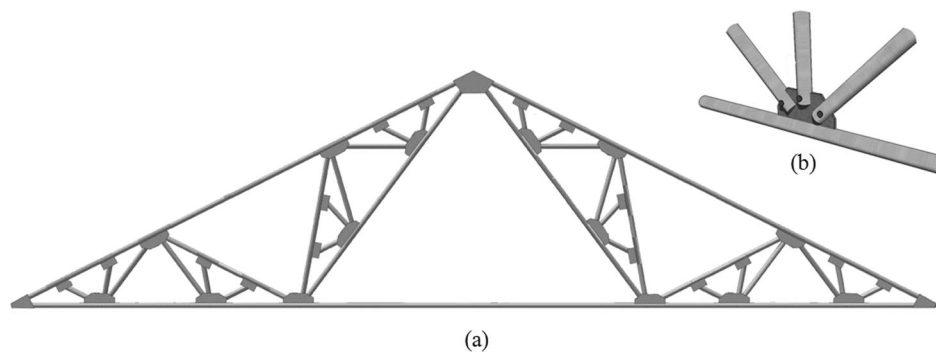


Figure 20. (a) An example of the architectural appearance of a fractal-based truss (Fan Fractal truss); (b) An illustration of a typical joint detail.

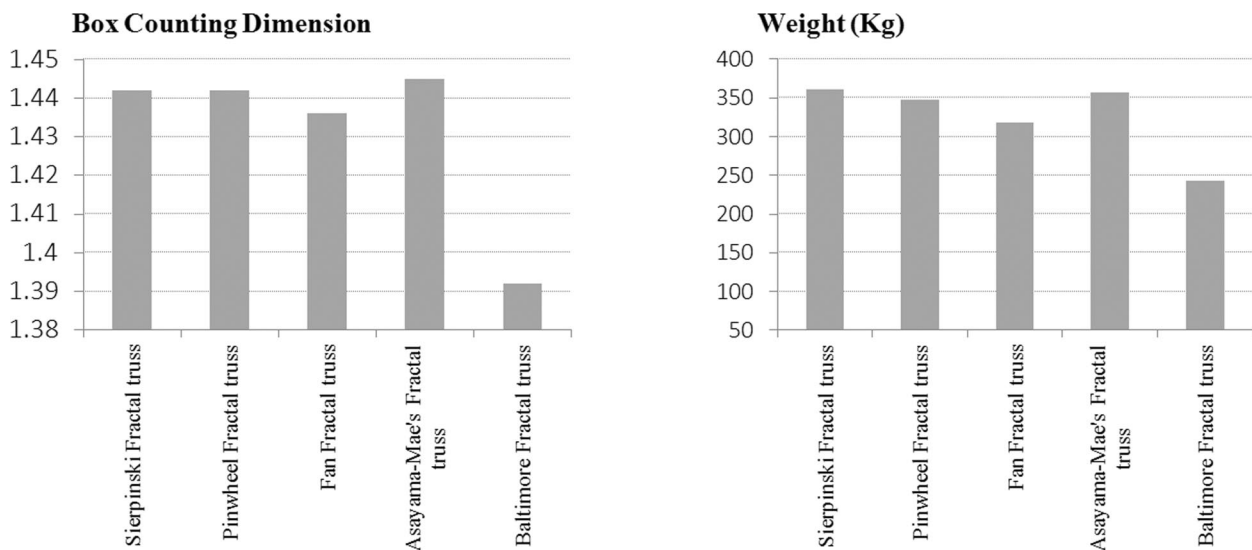
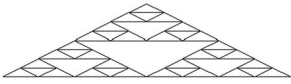






Figure 21. Comparison of Box Counting dimensions (left) and total weights (right) of different fractal-based trusses including conventional compound trusses when all the members have same cross-sectional area.

compromising the number of joints. Therefore, the four members, which carry no or the lowest axial forces after applied loads, can be chosen for the elimination to make the Pinwheel Fractal truss as an isostatic. As a result, the shape of final isostatic Pinwheel Fractal truss will lose its

fractal property of self-similarity, but can be addressed as a fractal-like. Hence, after the structural analyses, if we find some bars are inactive under some load conditions, then we can opt them out which will turn the shape of a fractal-based truss into a non-strict fractal.

**Table 1. Evaluation of the statical determinacy of fractal-based trusses**

Fractal-Based Trusses	No. of elements ( $b$ )	No. of nodes ( $j$ )	No. of unknown forces $F = (2 \times b) + r$ [ $r$ is number of reactions = 3]	No. of equations of equilibrium $E_q = (1 \times b) + (2 \times j)$	Relation between ' $F$ ' and ' $E_q$ '	Statically Determinate?
 Sierpinski Truss	81	42	165	165	$F = E_q$	YES
 Pinwheel Fractal Truss	81	40	165	161	$F < E_q$	NO (hyperstatic)
 Asayama-Mae's Fractal Truss	81	42	165	165	$F = E_q$	YES
 Fractal Fan Truss	63	33	129	129	$F = E_q$	YES
 Fractal Baltimore Truss	61	32	125	125	$F = E_q$	YES

## 6. STRUCTURAL ANALYSIS OF FRACTAL-BASED TRUSSES

### 6.1. Considerations and models for the analysis

In order to have a first understanding of the mechanical behavior of the fractal-based trusses, a linear static analysis under various load conditions has been performed. Before the analysis, it is assumed that all members of the truss are perfectly straight, all joints are frictionless and all loads and reaction occur only at the joints. Since all the fractal-based truss models are statically determinate, except the Pinwheel Fractal truss model, the stiffness of members does not influence the distribution of internal axial forces, while it has an effect on the nodal displacements. Further, the self weight of the trusses is not taken into account, being usually much smaller than the other loads, so that a unique kind of cross section is adopted for all the bars that form the trusses. Because the self weight is also an indicator of the amount of steel required for construction, and then of the cost, using the same cross section for all bars allows to evaluate this quantity directly from the total length of bars. As it has already been said before, the trusses are externally constrained with a hinge and a trolley, so that the global behavior is

analogous to the corresponding simply supported beam. In that way, the influence of large displacements on the internal stress state can be neglected and the linear static analysis is reliable. This fact has been confirmed by some non linear analyses, performed taking into account large displacements.

Three different load conditions are used in analysis: vertical uniform at the top, vertical uniform at the bottom and lateral load (Figure 22). The loads are applied as nodal loads and they are calibrated in order to have the same resultant and then to produce the same reactions when they are applied on different trusses. The total vertical load applied at top is 15 kN and at the bottom chord is 15 kN, and the total lateral load applied is 15 kN. All members are hollow tubes having 6 cm diameter and 3 mm thickness made of steel, and the Young's Modulus of each member is  $2.05 \times 10^{11}$  Pa and Poisson's Ratio is 0.3.

### 6.2. Analytical results and discussion

'Figure 23' shows the deformations of fractal-based trusses under nodal loads applied on the top rafters. The maximum nodal deformations ( $\delta_n$ ) of all the fractal-based trusses have been evaluated and their stiffnesses  $k = F/\delta_n$  have been compared in 'Figure 24',

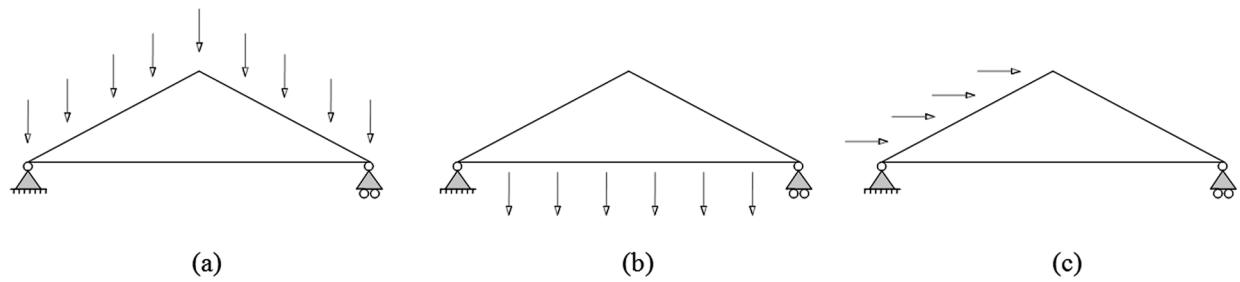


Figure 22. Different load cases; (a) vertical nodal loads applied on two rafters, (b) vertical nodal loads applied on the bottom chord, and (c) lateral nodal loads at one rafter.

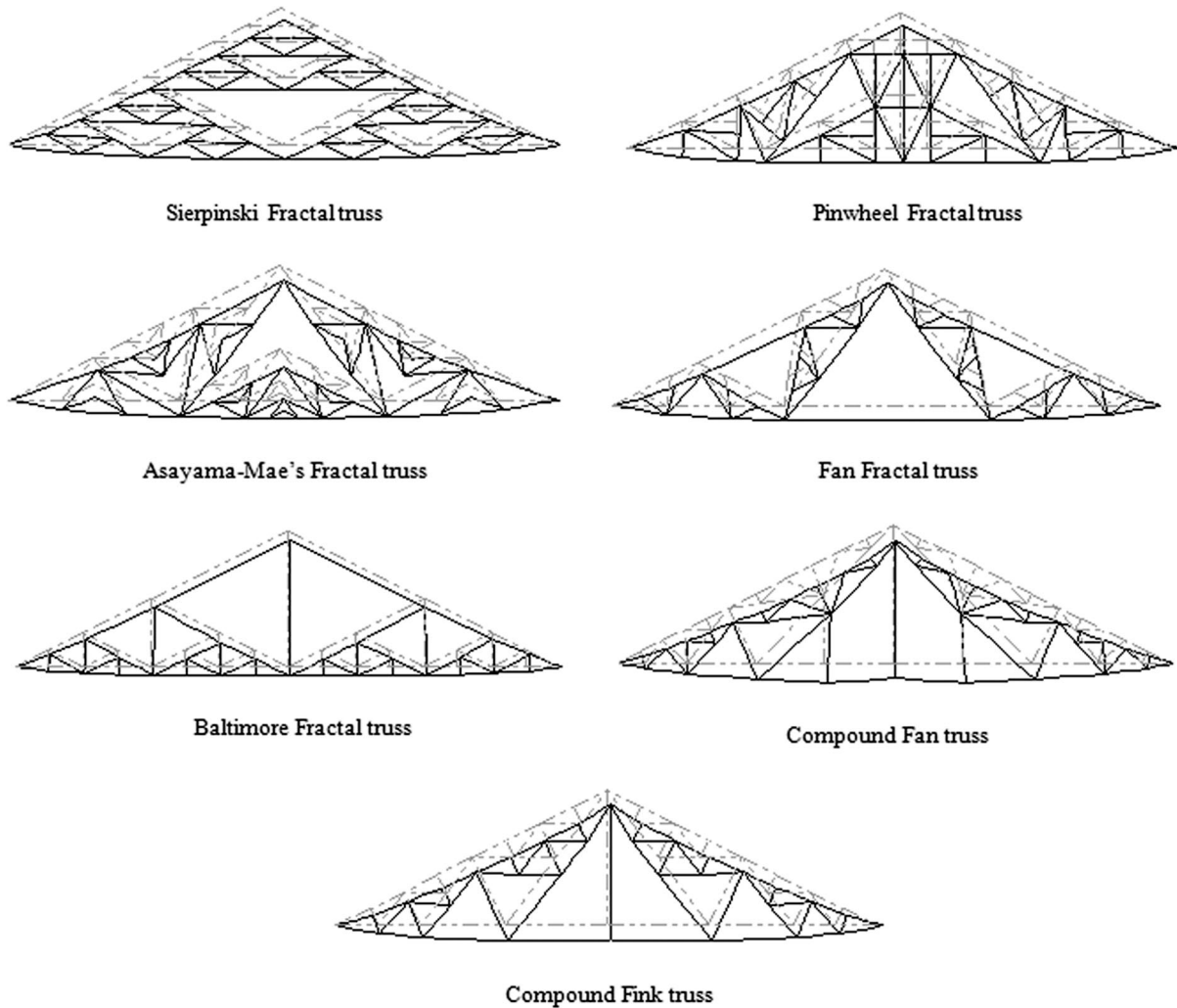


Figure 23. The deformations of fractal-based truss structures under vertical nodal loads applied on the top.

where  $F$  is the total force applied on the truss. We found that the maximum displaced node is not necessarily the top node. In this case the global behavior of each truss is analogous to the corresponding simply supported beam, because it is externally constrained with a hinge and a trolley. 'Figure 24, left' shows the differences between stiffness among the fractal-based as well as two conventional compound trusses. 'Figure 24, right'

is the Box Counting dimensions of the entire truss that express the detailness of internal lattices. By comparing these two figures in 'Figure 24', we notice that here is no significant relation between the stiffness and the detailness of a truss. For example, the Box Counting dimension of Baltimore truss is the lowest among others which means it is the least dense truss, but its stiffness is the highest among others. This

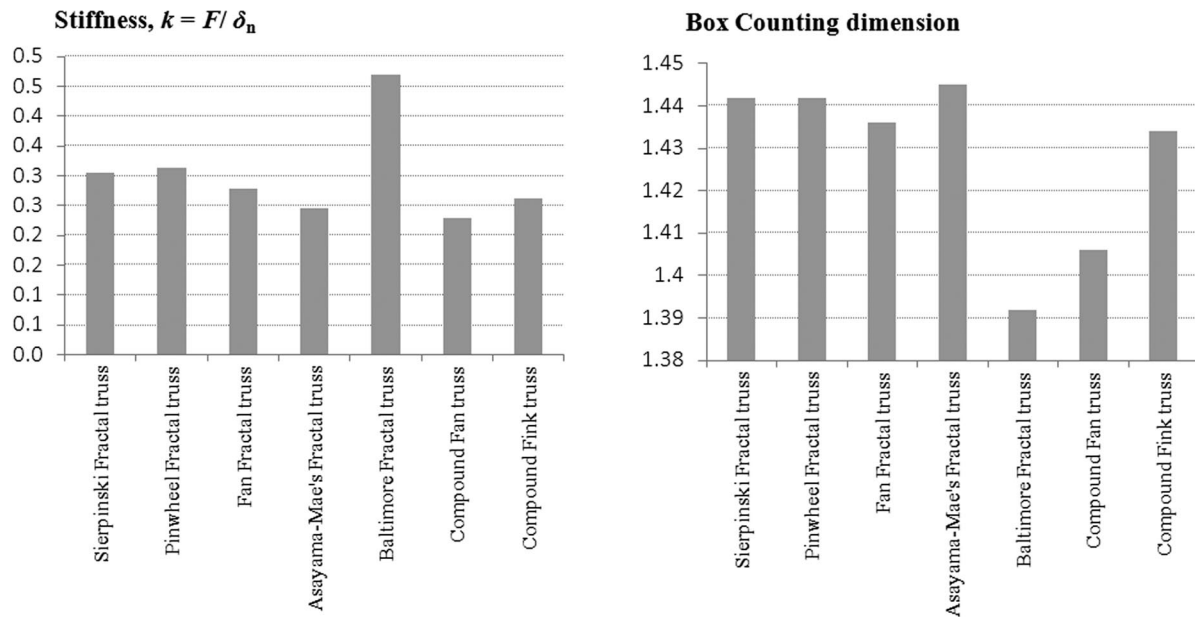


Figure 24. Left - The comparison of stiffness  $k = F/\delta_n$  of fractal-based trusses and conventional compound trusses, where  $F$  is applied forces and  $\delta_n$  is maximum nodal deformation; Right – Comparison of Box Counting dimensions of the truss structures.

comparison confirms that the density of internal lattices has no effect on the strength of the truss structures, instead, the strength comes from their design topologies. Hence, this structural behavior can be more clearly understood by analyzing the internal forces inside the truss.

The 'Figure 25a' and 'Figure 25b' show the internal forces, inside the Sierpinski Fractal truss, due to nodal forces applied on the upper rafters and on the lower chord, respectively. It is noticed in the 'Figure 25a' that the distribution of internal forces shows some extend of self-similarity nature. The presence of branching fractal patterns allows the application of different loads on the boundary of the truss, by stiffening its long straight sides. As for all the other cases, the flow of forces depends on the load condition, so that different parts of the structure are stressed under different loads. In fact, the most important feature of fractal's self similar subdivision is to reduce the size of the elements and to increase the number of nodes. Depending on the

load condition, some elements can be fully unloaded, because the force flow does not involve them.

If an element is never loaded under any load condition, it can be considered as redundant and the truss can be simplified by removing it. In general, every time a node links three elements two of which are aligned, the third becomes inactive, unless an external load is directly applied on the node. In practical cases, the imposed loads on a truss only act on the nodes on the boundary of the truss. Some variation of the reference fractal pattern, in order to avoid inactive elements, is shown in 'Figure 26a' and 'Figure 26b', from the Sierpinski fractal shape. In 'Figure 26a' is shown the simplified version with bottom load only, while in 'Figure 26b' the simplified version for top load. 'Figure 27a' and 'Figure 27b' show the corresponding modified versions for the Pinwheel fractal truss.

'Figure 28' shows the internal forces due to the combined three load cases 'a', 'b' and 'c' of 'Figure 22'.

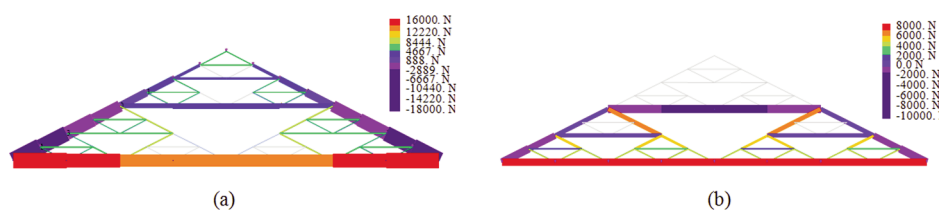


Figure 25. Internal forces in the Sierpinski Fractal truss; (a) Internal forces due to nodal forces applied on the upper rafters; (b) Internal forces due to nodal forces applied on the bottom chord.

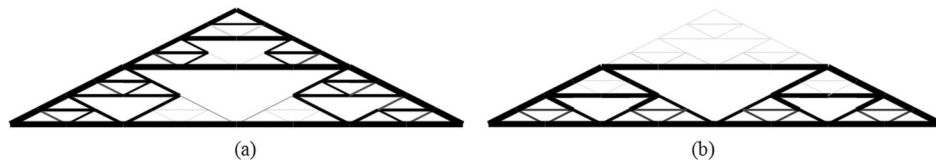


Figure 26. Reference fractal pattern of Sierpinski Fractal truss to avoid inactive members; (a) when applied vertical forces are on the top rafters; (b) when applied vertical forces are on the bottom chord.

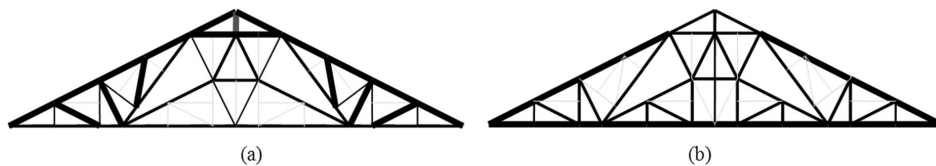


Figure 27. Reference fractal pattern of Pinwheel Fractal truss to avoid inactive members; (a) when applied vertical forces are on the top rafters; (b) when applied vertical forces are on the bottom chord.

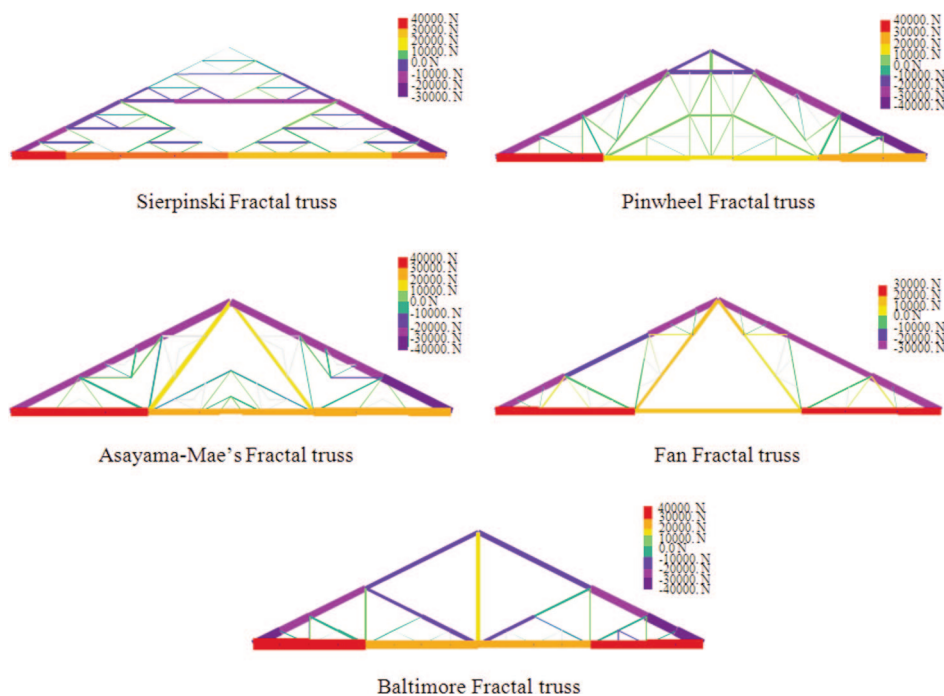


Figure 28. Axial forces in the fractal-based trusses under the combined three load cases 'a', 'b' and 'c' of 'Figure 22'. Green to blue and violet is under compression, and yellow to brown and red is under tension.

From the figure, we have noticed that almost most of the internal members are active under the combined loads, but some members do not experience any force, especially in the Pinwheel Fractal truss, Asayama-Mae's Fractal truss and Fan Fractal truss. The inactive members can be taken out which may transform the trusses statically indeterminate. But, from aesthetic point of view, and to keep the truss statically determinate, these inactive members can be kept as they are.

## 7. CONCLUSION

This paper has attempted to address the scope of applying the concept of fractal geometry in the field of construction aiming to introduce a new geometric system in designing structural trusses. The mathematical formulation called Iterated Function System has been applied to automatically generate the shapes of structural trusses as rule-based configurations. From the full mathematical definition



of the analyzed fractal configurations, it has been possible to evaluate their Hausdorff dimensions and their Box Counting dimensions. Based on this strategy, a set of new fractal-based structural trusses have been generated, in part as geometric refinement of more conventional schemes, in part as truly new designs. The definition of the abstract fractal geometry is just the first step of the design: the translation to real structures has required a set of adjustments as the substitution of all the two dimensional generating figures with segments, in some cases the removal of elements from the fractal pattern and in general the arrangements required to obtain statically determinate configurations.

The structural analysis shows that the self-similar fractal branching of trusses is suitable to make them able to carry almost distributed loads, on both the upper inclined rafters and on the bottom chord. The internal forces flows largely depend on the applied load condition and they suggest that new shapes can be derived from the fractal patterns. This is particularly interesting from the architectural point of view, because such new solutions can show aesthetical values and innovative appearance that make them suitable for real design applications. The analysis also informs that the lattice density, as a measure of Box Counting dimension, has no significant influence on the strength of truss structures. It is the truss topology by means of geometric configuration that can offer strength.

A more complete evaluation of the structural applicability will require the whole design of fractal-based trusses, including optimal sizing of members, design of joints and more refined stability analyses, in order to compare their performances with more traditional solutions. Hence, it would be fruitful to pursue further research about applying the fractals as a new geometric concept in designing and developing innovative structural systems, as well as finding the efficient shapes in a new but geometric way in the domain of architecture and construction.

## ACKNOWLEDGEMENT

This work was supported by the Politecnico di Torino's Doctoral Research Grant and Abroad Research Grant.

The authors are deeply thankful to Professor Shuich Asayama (Tokyo Denki University, Tokyo) for his initial contribution in developing the authors' understanding about fractal mathematics linked with designing structures.

## REFERENCES

- [1] Asayama, S. and Mae, T., Fractal Truss Structure and Automatic Form Generation Using Iterated Function System, *Proceeding of ICCCB E-X*, 2004; Weimar, Germany.
- [2] Barnsley M. F., *Fractals Everywhere*, Academic Press, Inc., 1988.
- [3] Batty M., *Fractals - Geometry between Dimensions*. New Scientist (Holborn Publishing Group) 105 (1450): 31, 1985.
- [4] Bovill, C., *Fractal Geometry in Architecture and Design*. Birkhauser, Boston, 1996.
- [5] Calvert, J. B., Truss Bridge Design: The History and Principles of Rational Truss Bridge Design, 2000, <https://mysite.du.edu/~jcalvert/tech/machines/bridges.htm>
- [6] Dekking M., et. al. eds., *Fractals: Theory and Applications in Engineering*, Springer, 1999.
- [7] Devany, R. L., *A First Course in Chaotic Dynamical Systems*. Reading, Massachusetts: Addison-Wesley Publishing Company, Inc., 1992.
- [8] Epstein, M. and Adeeb, S., M., The Stiffness of Self-Similar Fractals, 2008, *International Journal of Solids and Structures*, 45 (11–12), 3238–3254
- [9] Falconer, K., *Fractal Geometry, Mathematical Foundations and Applications*. 2nd ed. Wiley, London, 2003.
- [10] Gawell, E., Non-Euclidean Geometry in the Modeling of Contemporary Architectural Forms, 2013, *The Journal of Polish Society for Geometry and Engineering Graphics*, 24, 35–43.
- [11] Hutchinson, J. E., Fractals and Self-Similarity. *Indiana University Mathematical Journal*, 1981; 30 (5), 713–747.
- [12] Huylebrouck, D. and Hammer, J., From Fractal Geometry to Fractured Architecture: The Federation Square of Melbourne, 2006, *The Mathematical Intelligencer*, 28(4), 44–48.
- [13] Kishimoto, N. and Natori, M. C., Basic Consideration of Structures with Fractal Properties and Their Mechanical Characteristics, 2000, *Forma*, 15, 113–119.
- [14] Leung A. Y. T., Wub G. R. and Zhong, W. F., Exterior Problems of Acoustics by Fractal Finite Element Mesh, 2004, *Journal of Sound and Vibration*, 272, 125–135.
- [15] Leung A. Y. T., Fractal Finite Element Method for Thermal Stress Intensity Factor Calculation, *Proceeding of ICF11*, Italy, 2011.
- [16] Losa, G. A. and Nonnenmacher, T. F., eds., *Fractals in Biology and Medicine*. Springer. 2005.
- [17] Mandelbrot, B. B., *The Fractal Geometry of Nature*, W. H. Freeman and Co., New York, 1983.
- [18] Milne, B. T., The Utility of Fractal Geometry in Landscape Design, 1991, *Landscape and Urban Planning*, 21(1–2), 81–90.
- [19] Ostwald, M. J., Fractal Architecture: Late Twentieth Century Connections Between Architecture and Fractal Geometry, 2001, *Nexus Network Journal*, 3(1), 73.
- [20] Peitgen, H. and Jürgens H. S. D., *Chaos and Fractals: New Frontiers of Science*, 2nd ed. Springer, 2004.
- [21] Radin, C. and Conway, J., *Quaquaversal Tiling and Rotations*, preprint, Princeton University Press, Princeton, 1995.

- [22] Rayneau-Kirkhope, D., Mao, Y., & Farr, R., Ultralight Fractal Structures from Hollow Tubes, 2012, *Physical Review Letters*, 109(20), 204–301.
- [23] Rian, I. M., Park, J. H., Uk Ahn, H., and Chang, D., Fractal geometry as the synthesis of Hindu cosmology in Kandariya Mahadev temple, Khajuraho, 2007, *Building and Environment*, 42(12), 4093–4107.
- [24] Rian, I. M., Sassone, M., Tree-Inspired Dendriforms and Fractal-Like Branching Structures in Architecture: A Brief Historical Overview, 2014, *Frontiers of Architectural Research*, 3(3), p 298–323.
- [25] Rian, I. M., Sassone, M., Asyama, S., Fractal Shell Design Using Iterated Function System. *Proceeding of IASS-SLTE 2014: International Association of Shell and Spatial Structures*, 2014 Sept, Brasilia, Brazil.
- [26] Rinke, M. and Kotnik, T., The Changing Concept of Truss Design caused by the Influenced of Science. *ICSA 2010 - 1st International Conference on Structures & Architecture*, Guimaraes, Portugal, 2010, 559–561.
- [27] Sornette, D., *Critical Phenomena in Natural Sciences: Chaos, Fractals, Self-Organization, and Disorder: Concepts and Tools*, Springer Science & Business, 2004, 128–140.
- [28] Stotz, I., Gouaty, G. and Weinand, Y., Iterative Geometric Design for Architecture, 2009, *Journal Of The International Association For Shell and Spatial Structures*, 50 (1).
- [29] Vicsek, T., *Fractal Growth Phenomena*, 2nd ed. World Scientific Pub Co Inc., 1992.
- [30] Vyzantiadou, M. A., Avdelas, A. V., & Zafiropoulos, S., The Application of Fractal Geometry to the Design of Grid or Reticulated Shell Structures, 2007, *Computer-Aided Design*, 39(1), 51–59.
- [31] Wallace, D. F., Bookworm on KCRW, 1996, *Kcrw.com*. Retrieved 2010-10-17.
- [32] Yeomans, D. T., *The Trussed Roof*. Sclar Press, 1992.

